PROCESS MODELLING OF COATED ABRASIVE DISK GRINDING AS PART OF A ROBOTIC SOLUTION

by

Douglas Edward Ivers

SUBMITTED TO THE DEPARTMENT OF MECHANICAL ENGINEERING
IN PARTIAL FULFILLMENT OF THE REQUIREMENTS
FOR THE DEGREES OF

BACHELOR OF SCIENCE
and
MASTER OF SCIENCE

at the

MASSACHUSETTS INSTITUTE OF TECHNOLOGY

September 1985

Signature redacted

Signature of Author: _____
Department of Mechanical Engineering
September 1985

Signature redacted

Certified by: _____
Daniel E. Whitney
Thesis Supervisor

Signature redacted

Accepted by: _____
Ain A. Sonin
Chairman, Department Committee

PROCESS MODELLING OF COATED ABRASIVE DISK GRINDING AS PART OF A ROBOTIC SOLUTION

by
Douglas Edward Ivers

Submitted to the Department of Mechanical Engineering
in partial fulfillment of the requirements for the Degrees
of Bachelor of Science and Master of Science

ABSTRACT

The process of coated abrasive disk grinding was studied on a macro-process level, and the two most important output parameters, surface finish and metal removal rate, were modelled in terms of input parameters. A surface finish (R_a) theory was developed based on a single grit model, and corresponding data were gathered. Surface finishes in the range of 30 to 80 micro-inches were obtained from disks as rough as 16 grit. For the second parameter, volumetric metal removal rate, data were gathered which agreed with a linear model common to other types of grinding. This model states that metal removal rate is proportional to the power delivered to the grinding region.

Thesis Supervisor: Dr. Daniel E. Whitney
Section Chief
Charles Stark Draper Laboratory, Inc.
Cambridge, MA

Title: Lecturer in Mechanical Engineering

ACKNOWLEDGEMENTS

He who trusts in himself is a fool,
but he who walks in wisdom is kept safe.

Proverbs 28:26

I thank my advisor, Dr. Whitney, for his role in this research and in my education (Engineering Internship Program), and I thank the National Science Foundation (Grant No. MEA-8207167) for funding this research and my graduate year at MIT.

I also thank Alex Edsall and Matt Brown for writing software which I used extensively, and Kim O'Brion and Liz Hubauer for typing this document. Others who contributed in countless ways are Reginald Roderick, Don Seltzer, and Richard Ciliberto.

TABLE OF CONTENTS

LIST OF SYMBOLS

A	total cross-sectional area of weld bead
A_p	area of contact patch
A_r	cross-sectional area of remaining weld bead
b	length of weld bead
C_0, C_1	empirical coefficients in the linear $\dot{Q}$-Π relationship
d	depth of penetration of the grit in the R_a model
D	mass density of workpiece
F_N	normal force at the contact patch
F_t	tangential force at the contact path, $F_t = \sqrt{F_D^2 + F_L^2}$
F_p	the force on a grit which causes pull-out
$f(x)$	surface profile, used to compute R_a
g	number of grits cutting
h	height of weld bead
k	thermal conductivity
K_1, K_2	empirical coefficients in the linear Π-$\dot{Q}$ relationship
L	length of workpiece; or integration length
ℓ	base width of a groove
m	mass of an average cutting grit
Δm	change in mass of the workpiece due to one grinding pass

LIST OF SYMBOLS (cont.)

n	number of passes
p	length of the contact patch in the direction of $1/V_f T$
$\dot{Q}$	volumetric metal removal rate
R	radius of the disk
R_a	surface finish, or surface roughness (see eq. 4)
R_a^*	worst allowable R_a for the first grinding station
R_c	radius to center of contact patch
T	period of disk rotation
ΔT	rise in temperature due to one grinding pass
T_w	temperature of the workpiece
T_{cr}	critical temperature above which the strength of the material is degraded
t	thickness of a plate workpiece
t_c	cycle time of a given factory
t_o	non-grinding time
t_r	remaining cycle time of the last pass
V_b	total initial volume of the weld bead
V_c	cutting velocity of grits relative to workpiece
V_f	feed speed
V_g	grit velocity relative to the grinder, $V_g = \omega R_c$
α	thermal diffusivity
γ	half-apex angle of an average groove

LIST OF SYMBOLS (cont.)

Δ	see Δm, ΔT
δ	amount of disk deflection below the top of the bead
θ	inclination angle of grinder relative to workpiece
μ_c	composite coefficient of friction defined as F_t/F_N (not to be confused with μ in μm = micron = $10^{-6}m$)
Π	input cutting power
π	3.14159
ω	wheel speed <rad/s>

I. INTRODUCTION

In this thesis the volumetric metal removal rate (MRR) and the surface finish (R_a) in coated abrasive disk grinding (CADG) are analyzed in terms of easily-measured parameters. The approach is on a practical level such that only a few empirical coefficients are needed in the model equations.

In this chapter coated abrasives are introduced, and the automation of disk grinding is discussed.

A. General Information about Coated Abrasives

Similar to sandpaper, coated abrasives consist of a backing such as fiber re-inforced paper and a layer of grits embedded in (or coated with) a resin matrix. These hard grits are usually aluminum oxide. When a coated abrasive is rubbed on metal, tiny chips are formed as the grits cut grooves in the surface and remove metal. The region of contact between the coated abrasive and the workpiece is called the contact patch.

The two most common forms of coated abrasives are belts and disks. Belt grinding has been automated and, consequently, has been studied as a process.[1,2,3]

Disk grinding, on the other hand, has not been automated and has not been studied as a process. (The literature on belt grinding will provide useful information for our task.) Coated abrasive disks are used on hand-held grinders which are common in the body shop and the auto factory. Both disks and belts need a stiff rubber or plastic backing to transmit forces to the workpiece and, thereby, remove metal.

1. Comparison to other types of grinding

The most common type of grinding, surface grinding with vitrified wheels, is usually automated and has been studied widely. The grinding wheels are made by vitrifying (heating to 2300°F) a mixture of hard grits and other ceramics which form a solid, fused structure. Grinding with these wheels produces very smooth surfaces, but MRR (metal removal rate) is relatively low. Periodically the wheel must be "dressed" by scraping a diamond-tipped tool across the surface to expose fresh grits.

Another type of grinding, sometimes called snagging, uses resinoid-bonded wheels on hand-held grinders. An example of a snagging operation is smoothing the rough-cut edge of a thick steel plate. Resinoid-bonded wheels are similar to vitrified wheels except that no dressing is needed. Worn grits are continually torn loose during

grinding to expose fresh grits. A delicate balance of disk properties and grinding conditions determines the disk wear rate. A big issue, then, for automating this type of grinding is keeping the process in the efficient-grinding regime, that is, maintaining an optimal disk wear rate.(4)

Coated abrasive grinding, in contrast, has no self-renewal process or manual dressing. When the single layer of grits is worn, the disk or belt is thrown out. For this reason wear is an important phenomenon in coated abrasive grinding. It is discussed further in the next section.

CADG (coated abrasive disk grinding) is particularly suited to smoothing (removing lumps, burrs, or weld beads from) complex surfaces such as a car body. CADG can produce a "feather edge" on flat or curved surfaces. A feather edge is a very smooth transition between ground and unground regions on a surface.

Table 1 summarizes and quantifies the comparisons of this section.

TABLE 1. Comparison of different types of grinding in terms of typical grinding conditions.

	Vitrified Wheel Grinding	Resinoid Wheel Grinding (Snagging)	Coated Abrasive Disk Grinding
Tool support	machine	hand	hand
Workpiece shapes	flats, cylinders	edges, various shapes	complex surfaces
Wheel speeds	250 cps (15,000 rpm)	100 cps (6,000 rpm)	100 cps (6,000 rpm)
Contact force	500N (100 lbs)	70N (15 lbs)	30N (7 lbs)
Depth of cut	0.013 mm (0.0005")	1.3 mm (0.05")	0.13 mm (0.005")
Metal removal rate	5 mm^3/s (0.0003 in^3/s)	500 mm^3/s (0.03 in^3/s)	33 mm^3/s (0.002 in^3/s)
Surface finish	0.25μ (10 μ")	25μ (1000 μ")	5μ (200 μ")
Sharpening method	sharpening tool	self-renewing	change to a new disk

2. Wear of coated abrasives

Wear has traditionally been the biggest drawback of coated abrasives. In our research group **adaptive learning** is under investigation as a solution to this problem. Adaptive learning is a control technique which can adapt to a changing process by changing its model of the process. (Another solution would be to model the wear process, which many are trying to do for belt grinding.)

As the coated abrasive wears, MRR decreases and surface finish improves (R_a decreases). Three regimes of wear have been identified.[2,3] In the first few minutes of grinding, the coated abrasive goes through **initial rapid wear** in which micro-cracks within grits and weak bonds in the resin are broken. Once these fractures are over, **attritious steady wear** sets in. In this regime, the grit peaks decrease in height linearly with time and flats (parallel to the plane of the disk) form in their place. **Pull-out** occurs when the grits are worn down to the matrix which is destroyed, or when the force per grit is too high which is not economical.

The data in this thesis were taken in the attritions steady wear regime because it is the most stable. Disks in this wear regime are referred to as "worn in". Wear itself, however, was not studied in this thesis.

B. Automation: The Big Picture

This section describes the context of my work within the overall project to automate disk grinding.

1. Advantages of Automation

Coated abrasive disk grinding on car bodies has changed little in the past 75 years. Workers must wear layers of protective clothing and rest frequently. The situation is similar in grinding weld beads on ships.

Automation of this task offers several advantages over the present method. First, a large robot can push harder than a human operator and remove metal faster. Also the robot won't need frequent rest. Second, as we discovered in our research, surface finish can be improved by a factor of 10 with a uniform low feed speed and uniform normal force which a heavy robot can provide. This might eliminate one of, typically, three grinding stages of progressively finer grit. Third, a link to the CAD system of a factory is possible, which could provide better conformity of the product to its original design. Fourth, a dirty, tiring, dangerous job would be eliminated.

2. Project goals

The goals of our overall research project are (a) to investigate adaptive learning and its application to CADG, (b) to build an automated CADG system that will remove silicon-bronze weld beads from car bodies leaving an acceptable finish, and (c) to investigate automating resinoid wheel grinding or snagging. This thesis falls under goal (b).

C. Requirements of a Disk Grinding System

This section discusses the minimum requirements for a general disk grinding system on the process level.

1. Volumetric metal removal rate (MRR)

The system must remove a given amount of metal within the time constraints of production. Moreover, the system must be able to remove lumps and high areas, and avoid low areas. This will be accomplished if the system can control both the location of metal removal (see section 5) and the rate of metal removal. In the case of grinding a weld bead on a car body, MRR on the last pass is crucial because a slight overshoot (MRR too high) would damage the 1/32 inch thick steel body.

How can the instantaneous MRR be measured by the system? Various methods were considered for study such as measuring the volume, mass, or momentum of the removed chips. In other types of grinding, MRR is linearly related to the cutting power Π (force times velocity - not electrical power) delivered to the contact patch.[4,5] If this holds true for CADG, then MRR can be measured instantaneously with a force sensor and tachometer. Part of the objective of this thesis is to see if MRR is linear with Π in CADG.

2. Disk wear parameter (DWP)

The system must know or decide when to change to a new disk. (This section concerns DWP for CADG only. See ref. 4 for a description of DWP in snagging.) If it is economical to use the disk until it falls apart, then an indicator might be the composite coefficient of friction μ_c defined as the tangential force divided by the normal force.

I suspect, however, that it will be economical to change the disk much sooner. In this case, the logical parameter to use is the output divided by the input, that is, MRR divided by the input cutting power Π. If MRR, $\dot{Q}$, is linear with Π then the slope of the line C_1 could be considered the DWP. Mathematically,

$$\dot{Q} = C_o + C_1 \Pi$$

$$C_1 = \{DWP\}.$$

C_1 may depend on grinding conditions other than wear, but over a long period of grinding, the trend in C_1 due to wear could be detected. Although confirming this hypothesis is beyond the scope of this thesis, in early experiments with a new disk, C_1 dropped sharply (corresponding to initial rapid wear) and then leveled off to a much slower rate of change (corresponding to attritions slow wear).

3. Workpiece temperature

The temperature of the workpiece must not get too high, or the strength of the joint will be degraded. A crude analysis (see Appendix D for derivation) reveals the following relation for thin plates:

$$\Delta T \approx \frac{\Pi}{2kt} \sqrt{\frac{\alpha p}{\pi V_f}}$$

where ΔT is the maximum rise in temperature due to one grinding pass. Once again the cutting power Π seems to be an important quantity, along with the feed speed V_f, plate thickness t, contact patch length p, and material properties, k and α. Of course, if a cooling fluid is

used, convective heat transfer becomes significant and the above relation is not applicable.

4. Surface finish

The surface finish is often important only to an order of magnitude. The criterion for car bodies is that the ground region not be dectable visually or tactually after the car has been painted. The grinding system must be able to meet such requirements.

Surface finish R_a is expected to be a function of feed speed V_f, wheel speed ω, normal force F_N, and disk properties such as grit size. The finish is expected to be a function of cutting power only to the extent that power is a function of the above parameters. A theoretical model is derived in Section II.B.

5. Contact patch location

The system must be able to remove metal from the right areas of the workpiece. More specifically, the location and height of lumps and high areas with respect to the parent surface or some desired surface within the workpiece must be detected relative to the disk. This can be accomplished during grinding with a 6-axis force sensor.(6) For the remainder of this section, the issue is discussed in terms of weld bead grinding.

The position of the weld will be known within an inch or two **a priori** with proper jigging. The disk, which is typically five inches or larger in diameter, could be lowered to the workpiece and always contact the weld bead. During grinding, the location of the contact patch on the disk - thus the location of the grinder relative to the bead - can be measured by a force sensor. Using feedback, the system can center the contact patch and track the bead during the grinding pass.

Currently in our group at Draper, a vision system is being developed to measure the profile of the bead across the joint as shown in Figure 1a. This system will be able to find the best contact patch location. If the grinder is not in the correct location, the ground flat on the bead will be slanted as shown in Figure 1b. The vision system will be able to detect this and instruct the grinder to move accordingly. When the bead has a flat that is parallel to the parent surface as in Figure 1c, then the grinder is in the correct lateral position.

Finally, the size and shape of the contact patch may be important in some cases. For example, even if the disk is centered on the bead, some part of the disk may also be touching the parent surface. This could seriously damage a car body. One way of monitoring this is to detect the sparks that occur when grinding steel. (Silicon bronze doesn't spark.)

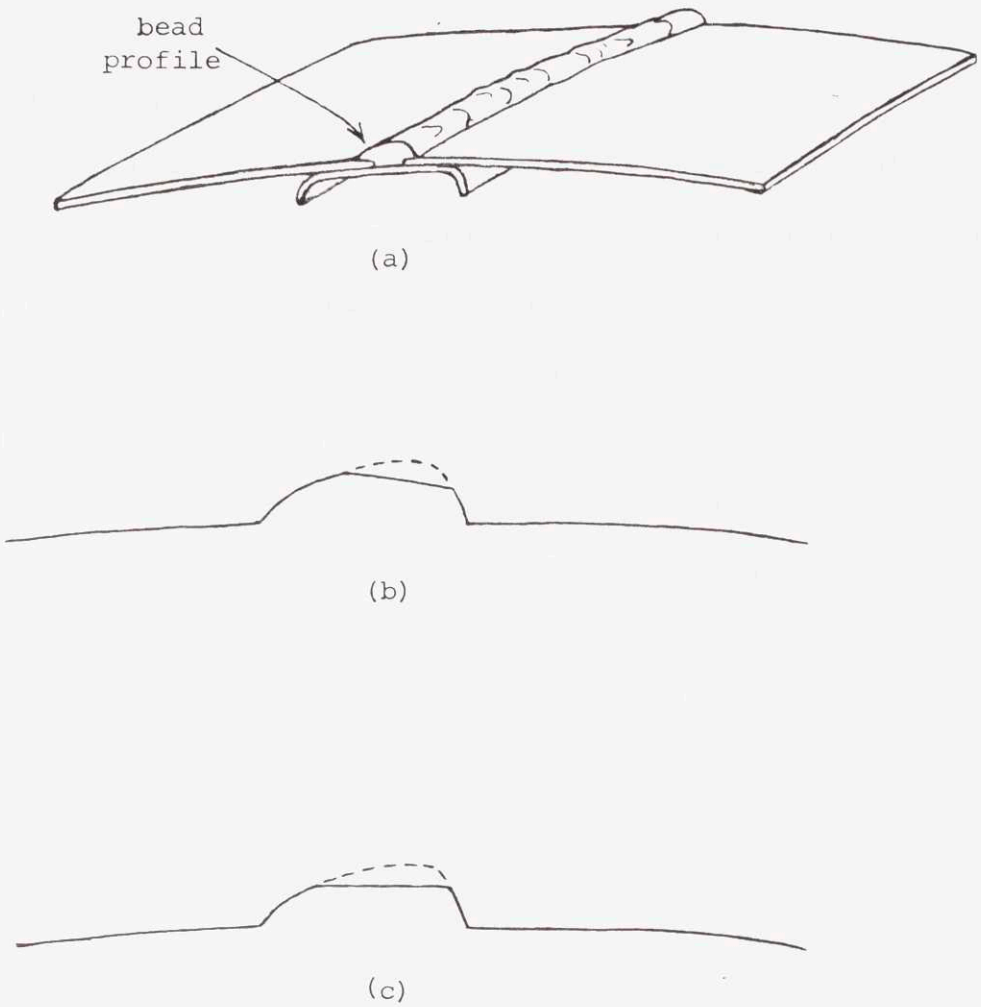

Figure 1. (a) Bead profile which will be measured by the vision system.

(b) Profile of a bead ground by a disk grinder which was too far to the right.

(c) Profile of a bead ground by a disk grinder in the correct lateral position.

D. Summary

Based on what an automated system must accomplish, five output parameters were developed. Since it is difficult to measure any of these parameters directly, some modelling of the process is necessary. In other words, equations are needed that relate the output parameters to variables which can be measured. Such variables are called input parameters. According to our discussion, cutting power Π appears to be an important input parameter.

Figure 2 is a schematic of the CADG process with inputs and outputs. Most of the possible input parameters will be discussed in later chapters. The orientation, in particular, is explained in Appendix A.

POSSIBLE INPUT PARAMETERS	"UNKNOWN" PROCESS	OUTPUT PARAMETERS
forces		
wheel speed, ω		
cutting power, Π		
feed rate, V_f		
grit size		
other disk properties		
disk-backing properties		
orientation		
workpiece properties		
bead profile, bead width		
cooling fluid		

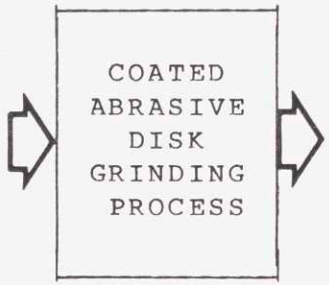

MRR, volume metal removal rate

R_a, surface finish

location of contact patch

DWP, disk wear parameter

temperature of the surface

Figure 2. Process Parameters

II. THEORETICAL ANALYSIS

This chapter discusses the MRR-power relationship, and derives an equation for R_a based on a single-grit geometric model.

A. Metal Removal Rate (MRR)

As mentioned earlier, in other types of grinding such as surface grinding and snagging, experiments show that MRR, $\dot{Q}$, is a linear function of cutting power Π. That is,

$$\dot{Q} = C_0 + C_1 \Pi \qquad (1)$$

in which C_0 and C_1 must be determined empirically.

If C_0 and C_1 turn out to be functions of forces or feed speed, then the model must be revised to include these parameters because they are integral to the control of the process. In particular, in order to grind a lumpy weld bead so that the finished surface is flat, the grinding system must control the metal removed along the bead by varying the normal force and/or feed speed (or, possibly, wheel speed) along the bead. The controller must therefore have a model equation for MRR which is valid under these changing conditions. Furthermore, whatever else C_0 and C_1 might depend on significantly must remain constant between calibrations, or else change slowly so that the system can

adapt. Attritious steady wear is expected to fall into the second category.

The MRR experiment described in the next chapter is designed to find any dependency of C_o or C_1 on feedspeed or normal force.

The cutting power in equation 1 is defined as

$$\Pi \equiv \left| F_t V_c \right|$$

The tangential cutting force F_t, which lies in the plane of the workpiece surface, is the sum of forces acting on the individual grits. The cutting velocity V_c is the average velocity relative to the workpiece of the grits that are cutting. Because V_f (feed speed) is much less than V_g (grit velocity relative to the grinder),

$$V_c \approx V_g = \omega R_c$$

ω - Wheel disk speed <rad/s>

R_c - Radius to center of contact patch <m>

Equation 1 can now be written

$$\dot{Q} = C_0 + C_1 \left| F_t \omega R_c \right| \qquad (2)$$

F_t, and ω are measured with a force sensor and

tachometer, while R_c was assumed constant - a maximum error of 4%.

For a better intuitive understanding of this model consider the following equation (derived in Ref. 7) which is equivalent to equation 1:

$$\Pi = K_1 \dot{Q} + K_2 \qquad (3)$$

in which

$$K_1 = 1/C_1$$

$$K_2 = -C_0/C_1.$$

K_2 is always positive or zero. Physically this means that it is possible to deliver power to the workpiece without removing metal. At this low power, the grits scratch the surface, but no chips are formed. K_2 is called the wasted power and, in typical grinding conditions, is small compared to $K_1 \dot{Q}$.

B. Surface Finish (R_a)

In early experiments at low feed speeds, the ground surface was surprisingly smooth. The grinding geometry of these experiments is illustrated in Figure 3a. A look through the microscope revealed very uniform and evenly

spaced grooves that one would expect from a single-point tool, instead of grinding. The average distance between these grooves was the distance the disk moved in the feed direction during one disk rotation. The hypothesis is that, though many grits are removing metal, the last grit that cuts largely determines the surface at very low feed rates.

To model this hypothesis, consider a single conic grit of apex angle 2γ which cuts grooves in the surface. With each revolution of the disk another groove is formed spaced from the previous one by a distance equal to the feed speed V_f multiplied by the period of rotation of the disk T as shown in Figure 3b.

R_a, which is the most widely used measurement of surface finish, is defined as

$$R_a \equiv \frac{1}{L}\int_0^L \left| f(x)-m \right| dx \qquad (4)$$

in which

f(x) - surface profile

m - mean of f(x)

L - integration length.

For periodic functions, L is the length of the smallest repeating unit. Putting the ground surface profile of

Figure 3b into this equation gives (with $L = V_f T/2$) the result:

$$R_a = V_f T/8\tan\gamma \qquad (5)$$

The depth d of penetration into the "unground" surface (which, in reality, has its own grooves from other grits) depends on the forces on this grit. As $V_f T$ increases, the surface becomes rougher according to the above equation. For $V_f T > \ell$ (where $\ell = 2d \tan\gamma$), however, the equation no longer applies. This situation is shown in Figure 3c. Replacing $\tan\gamma$ with $\ell/2d$ and solving equation 4 for the new surface gives, along with equation 5,

$$R_a = \begin{cases} \dfrac{V_f T}{8\tan\gamma} = \dfrac{d}{4}\left(\dfrac{V_f T}{\ell}\right) & \text{for } V_f T < \ell \\ \left[\left(\dfrac{\ell}{V_f T}\right) - \left(\dfrac{\ell}{V_f T}\right)^2 + \dfrac{1}{4}\left(\dfrac{\ell}{V_f T}\right)^3\right] d & \text{for } V_f T > \ell \end{cases} \qquad (6)$$

This equation is plotted non-dim. in Figure 4a. The effect of increasing d is shown in Figure 4b. The depth d will probably be proportional to the normal force.

Note that the model will not be accurate for large $V_f T$ (small $\ell/V_f T$) because a perfectly smooth "unground" surface is assumed. In reality, grooves from other grits will appear in the surface.

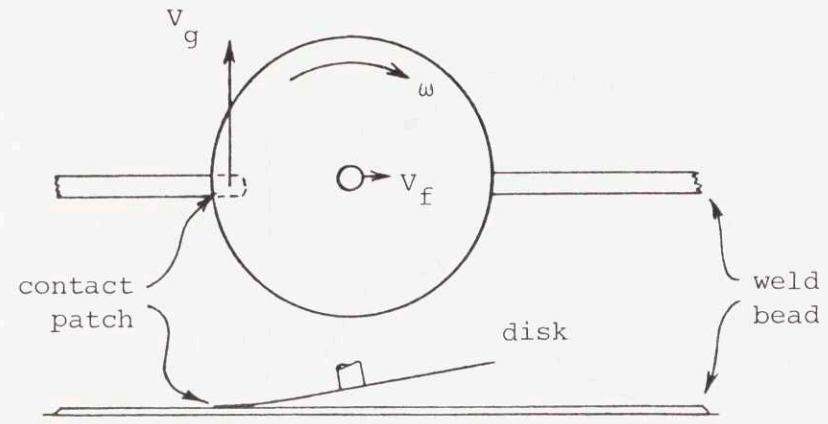

(a)

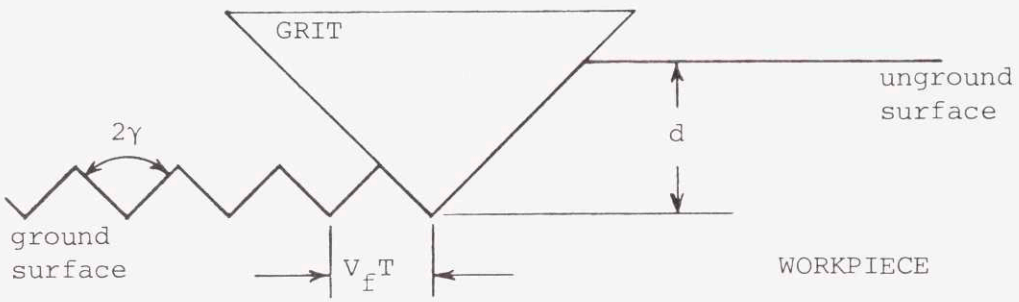

(b)

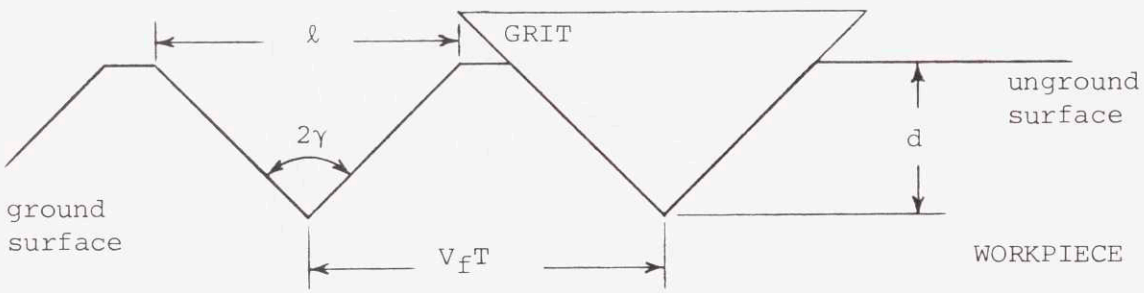

(c)

Figure 3. Surface Finish Model.

(a) Grinding geometry.

(b) Single-grit model for $V_fT < 2d \tan\gamma$

(c) Single-grit model for $V_fT > 2d \tan\gamma = \ell$

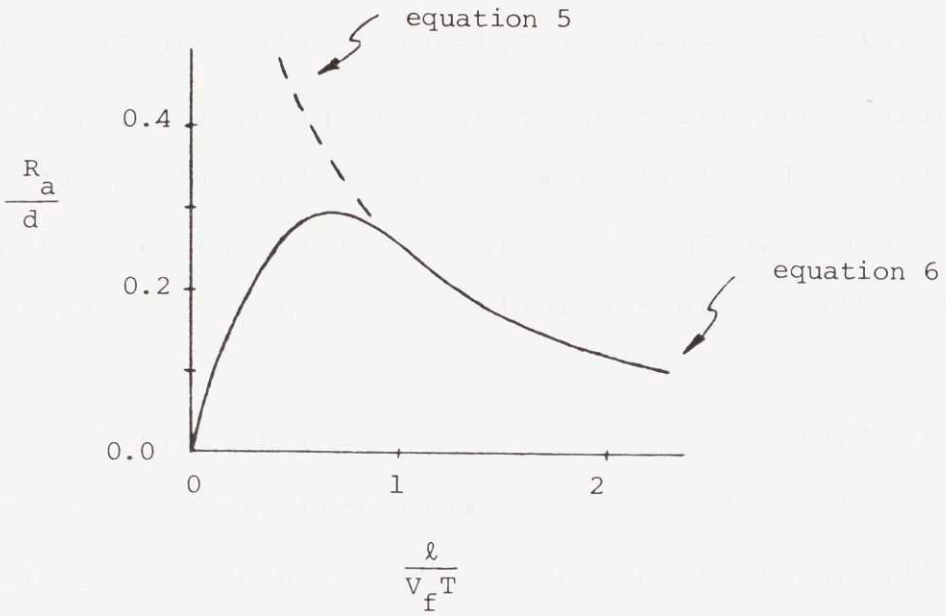

(a)

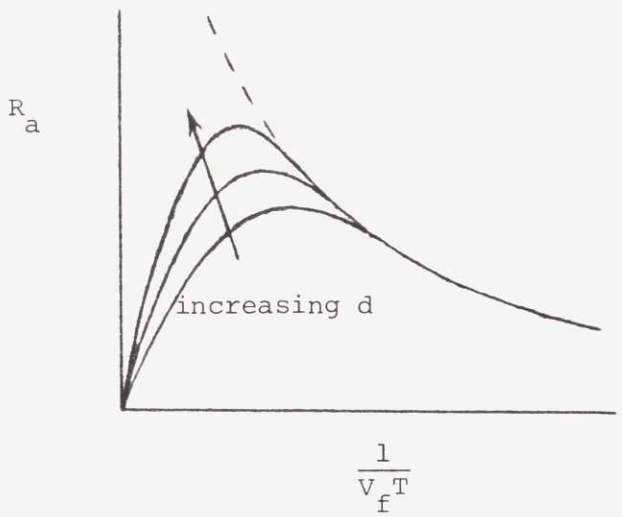

(b)

Figure 4. Surface finish model
(a) non-dimensionalized graph
(b) regular plot showing dependence on d

Experiments were conducted to evaluate γ and d for six different grit sizes (section III.C.). Some investigators [3,8] have designed systems to automatically measure average properties of coated abrasives and to arrive at statistical coefficients such as γ and d. Such a system could become part of the grinding system calibration.

Further, if γ and d are evaluated periodically (e.g., after each car), then equation 6 should account for wear because γ has been shown to increase with wear.[8]

III. PROCEDURE

These experiments were designed to find the relationship betweeen MRR and Π, and to test the R_a model developed in the previous chapter.

A. Overview of Apparatus

This section describes components of the experimental apparatus common to all the following experiments. Further detail can be found in Appendix B.

The milling machine equipped with a power feed table shown in Figure 5, was used as a test bed - a very rigid one-degree-of-freedom robot. The wooden box retained chips and muffled audible noise.

The 3-horsepower Milwaukee grinder shown in Figure 6 was instrumented with a 6-axis force sensor and high precision tachometer. The force sensor (partially obstructed) was mounted rigidly in the milling machine collet (hidden from view). The grinder, in turn, was mounted to the force sensor via shock mounts. The tachometer (hidden from view) was mounted between the disk shield and the disk.

A Variac (variable voltage regulator) was used to adjust the voltage on the grinder, which indirectly

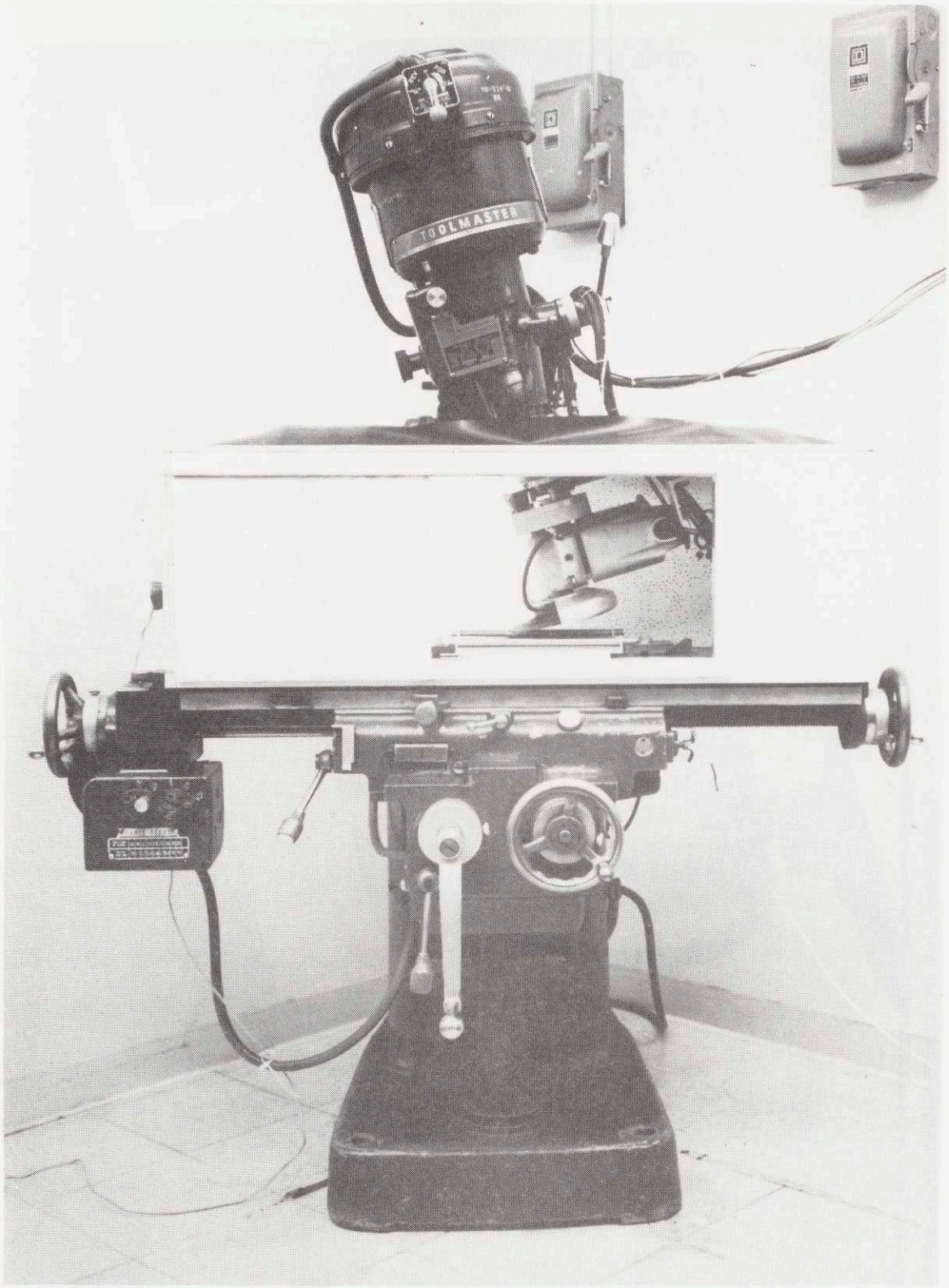

Figure 5. Milling machine test bed.

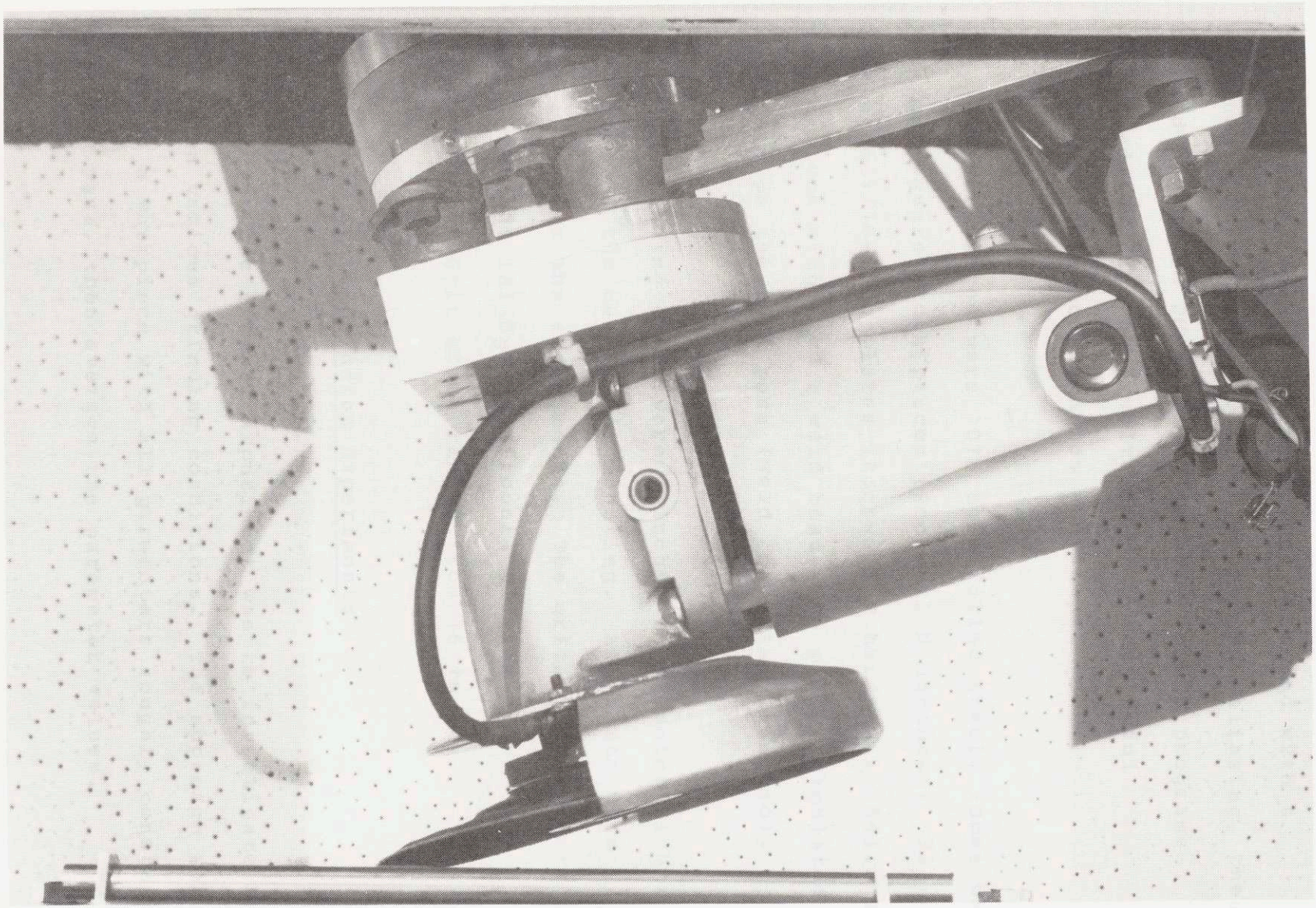

Figure 6. Instrumented grinder

determined the no-load disk speed.

The force sensor voltages were filtered with a 6-channel 10 Hz low-pass filter to prevent aliasing, then sampled by an IBM PC at 25 to 100 Hz. BASIC programs converted the digitized voltages into meaningful information using calibration equations.

All workpieces were 1018 cold rolled steel. Some were 1/2-inch square stock pieces (Rockwell B hardness: 93); some were 1/16-inch plates (Rockwell B hardness: 54). The square stock simulated a weld bead; the plates simulated the workpiece on the last pass (weld completely removed).

The grinding disks were 7 inches in diameter with a 7/8" hole in the center for mounting. All disks were worn-in before the experiments. The grits were either aluminum oxide (Al_2O_3) or zirconia alumina (Al_2O_3-ZrO_2). Grit sizes ranged from 16 to 80.

B. Steady State Grinding Experiments

The purpose of this experiment was to investigate MRR and R_a in various grinding conditions. The approach was to grind a workpiece with all parameters roughly constant over the pass, then average the parameter values.

1. Apparatus

The milling machine power feed provided constant feed speeds from 1.1 to 15 inches per minute. A magnetic chuck was used to hold each 1/2"-square-by-6"-long workpiece to the table. The height of the workpiece relative to the grinder indirectly determined the normal force. This is called the depth of cut in Figure 7.

Two different 36-grit disks and two different backings were used. A photodetector triggered the sampling program when grinding reached steady state (after about 1/2 inch of grinding). Figure 8 is a schematic of the data gathering system.

The workpiece was weighed before and after the pass so that MRR could be computed using the following equation:

$$\dot{Q} = \frac{\Delta m \; V_f}{DL}$$

$\dot{Q}$ - MRR

Δm - change in mass

D - mass density

V_f - feed speed

L - length of workpiece

The mass density of a typical workpiece was measured with the scales and calipers.

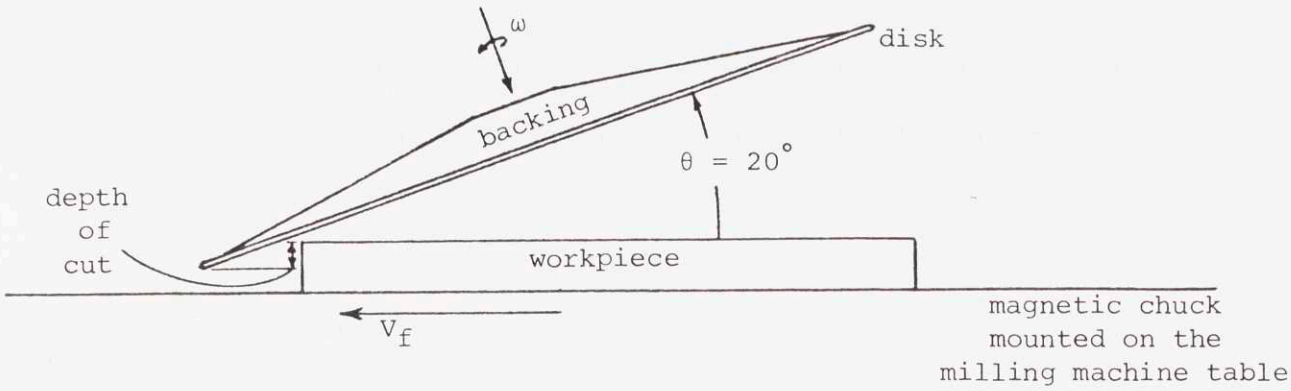

Figure 7. Geometry of the steady state grinding experiment in the starting position. Because the disk and backing deflect, the actual change in workpiece thickness due to a grinding pass is a small fraction of the depth of cut.

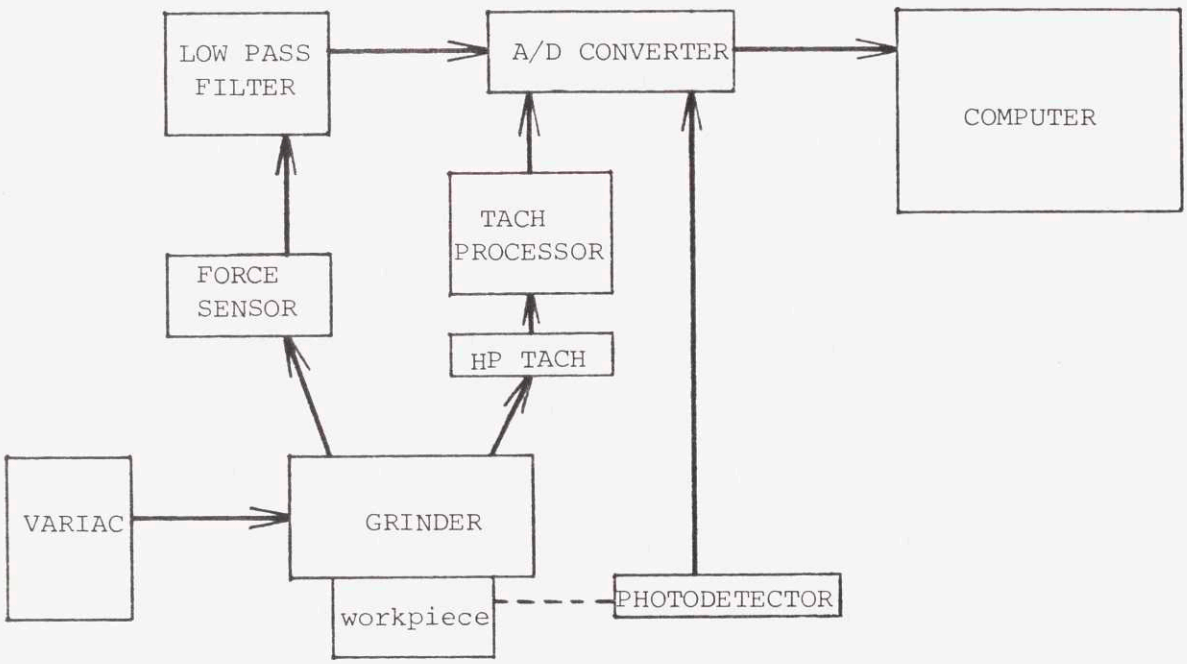

Figure 8. Data gathering system for the steady state grinding experiment. Not included in this schematic are the scales for MRR and the Surtronic 3 for R_a.

R_a was measured in several places on the workpiece with the Surtronic 3, a surface finish measurement instrument.

2. Procedure

The following describes the step-by-step procedure of one grinding pass which results in one mean datum of each parameter. The force sensor and the high precision tachometer were calibrated before the experiment.

a. Weigh the workpiece.
b. Place the workpiece on the magnetic chuck.
c. With the milling machine cranks, position the workpiece under the grinder at a depth of cut (see Figure 7).
d. Turn up the Variac until the tachometer output reads -1.32 volts (about 5400 rpm).
e. Monitor the force sensor until warmed up.
f. Load the sampling program and sample the force sensor output for offset values.
g. Start the feed table. Sampling automatically begins when the disk is fully on the workpiece and ends five inches later.
h. Weigh the workpiece again.
i. Collect chips (not analyzed in this thesis) from the chuck, then wipe it clean.

j. Measure R_a in several places.

k. Type MRR and the average R_a into the computer. Store these along with average parameter values.

This procedure was repeated at different depths of cut and feed speeds.

C. Grit Parameter Experiment

This experiment finds the average grit parameters, γ and d, for six disks of different grit sizes. The approach is to measure profiles of individual grooves - not the grits themselves.

1. Apparatus

The experimental set-up is essentially the same as before - except there is no feed, and the workpiece is a flat plate. The Bendix Proficoder and the Dektak II were used to measure individual grooves.

2. Procedure

The following procedure was conducted for 16, 24, 36, 50, 60 and 80 grit disks at roughly the same normal force.

a. With the wheel stationary, sample the force sensor for offsets.

b. Start the sampling program manually.

c. Center the plate workpiece under the tip of the disk.

d. Raise the workpiece into the disk to some depth (wheel still stationary) such that the contact patch is in the middle of the workpiece.

e. Turn on the Variac, increasing the voltage until the disk breaks free and begins to rotate.

f. Immediately turn off the Variac, allowing the disk to rotate only about one revolution.

g. Lower the workpiece from the disk.

h. Record the surface profile across the grooves. An example is shown in Figure 9.

i. Imagine fitting an isosceles triangle to each groove as illustrated in Figure 10. Record the dimensions of the idealized groove.

j. Average the dimensions of the seven largest grooves.

The rationale behind only averaging the seven largest grooves is that the grit which forms the final surface will be a large one near the perimeter. One could take this idea further and use a weighting function which favors grits near the perimeter. This, however, was not done in this study.

D. Quasi-Steady State Grinding Experiment

The purpose of this experiment was to get more data per pass and to use the higher feed speeds of a new feed table.

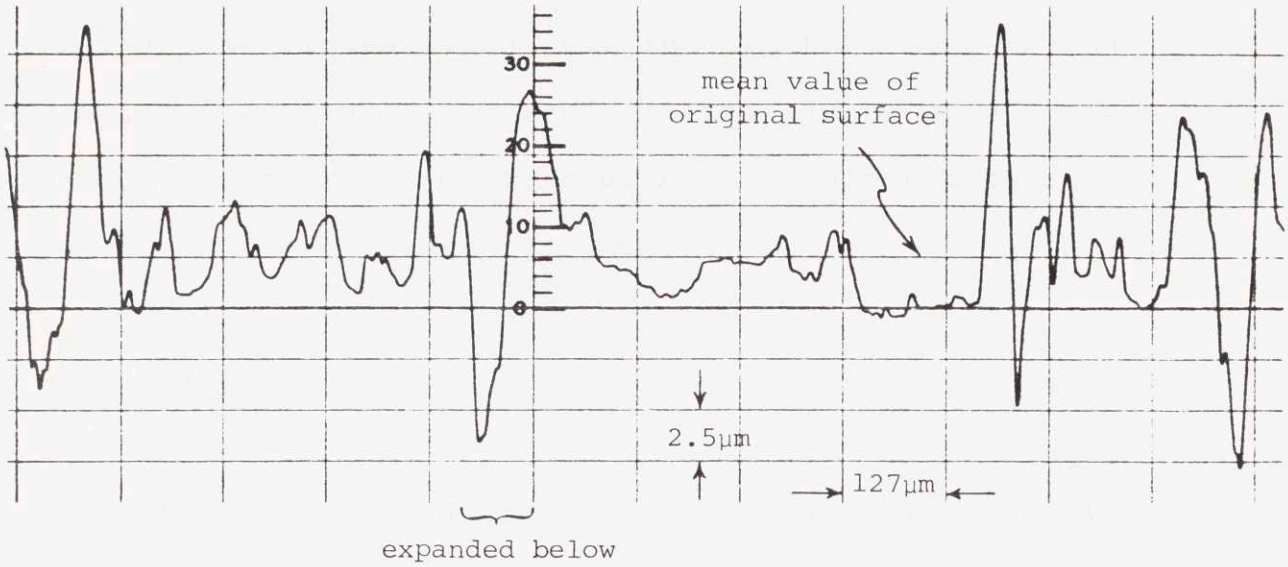

Figure 9. Part of a surface profile of individual grooves. Output is from Bendix Proficoder.

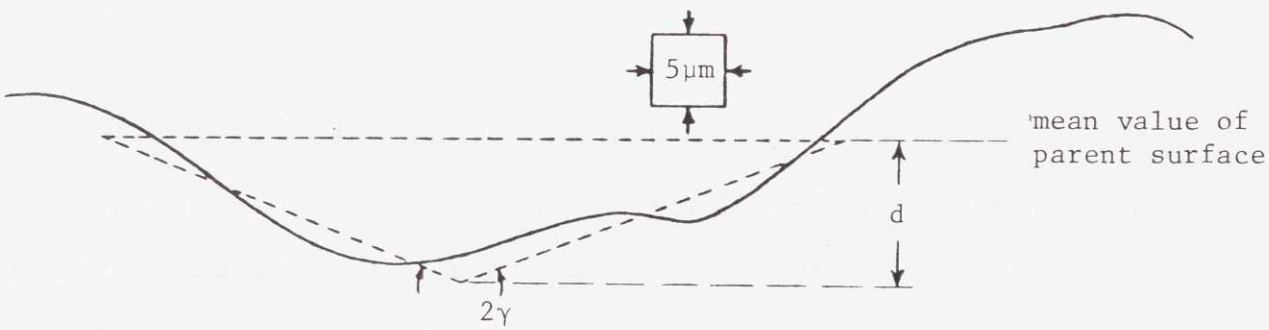

Figure 10. Expansion of second groove above. Heavy dotted line is an example triangular fit. In this way γ and d are found for the 7 largest grooves and averaged.

The approach was to incline the workpiece slightly as indicated in Figure 11 so that the depth of cut, normal force, and cutting power were all increasing slowly over the pass. Parameters were averaged over 1/2-inch intervals yielding 15 data points per pass.

1. Apparatus

The new fast-feed table (5 in/s maximum) was equipped with a D.C. tachometer which triggered the sampling program as well as measured the feed speed of the table. A sloped fixture of 1.64° was mounted on the table. Although the workpieces were 10" long, data was extracted between 3/4" and 8 1/4" along the workpiece in order to avoid end effects.

In these experiments MRR was separated from R_a. The R_a experiment was conducted by grinding flat plates, which better simulates the last pass in bead grinding. (R_a is not important until the last pass.)

The MRR experiment was still conducted on square stock, but MRR could no longer be measured by weighing the workpiece. The new approach was to measure the change in cross-sectional area of the workpiece (multiplied by the feed speed equals MRR) at 1/2" intervals using a precise electronic displacement indicator. These measurements were made both before and after the grinding pass. As shown in

Figure 12, the workpiece was clamped to the magnetic chuck to insure that the workpiece was "seated" every time. (The steel might bow slightly due to grinding.)

The new measurement system is shown schematically in Figure 13.

2. Procedure - increasing force

First the D.C. tachometer was calibrated, and the force sensor and high precision tachometer were recalibrated. Then the following procedure was executed for various feed speeds. (Note that some items are for the MRR experiment only; others, for the R_a experiment only.)

a. For MRR, measure the thickness of the new workpiece down the middle (length-wise) and across the width. (Square stock is not perfectly flat across the width.)
b. Mount the workpiece and position it under the grinder for a small initial depth of cut. (See Figure 11.)
c. Turn on the grinder to full speed.
d. Load the sampling program while the force sensor warms up. Set the desired feedspeed.
e. Sample the force sensor for offsets.
f. Start the feed table, which triggers the sampling program.

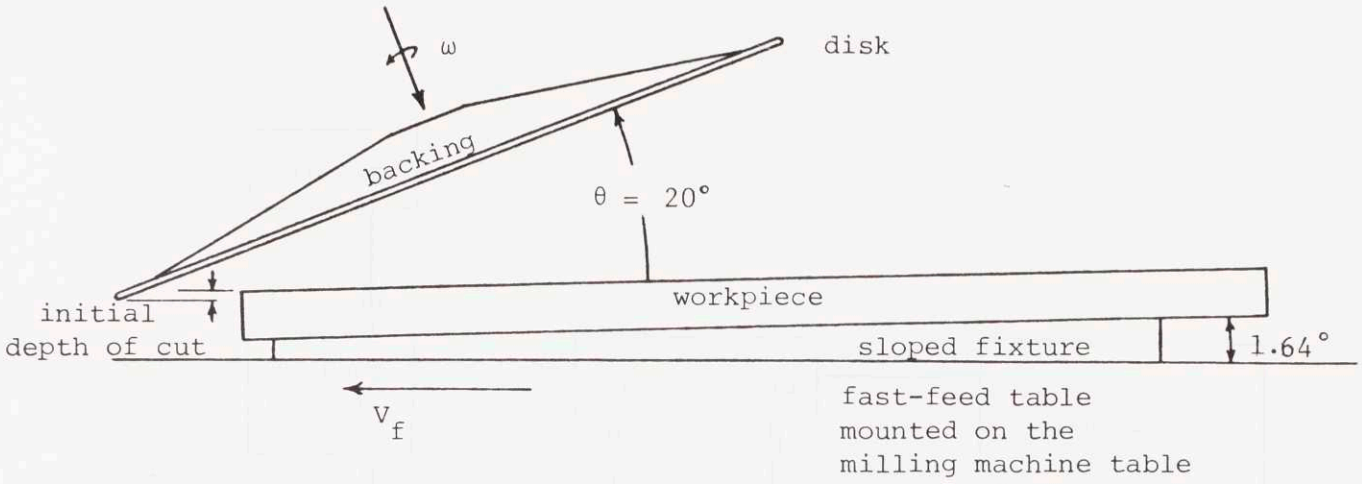

Figure 11. Geometry of Quasi-steady State Grinding

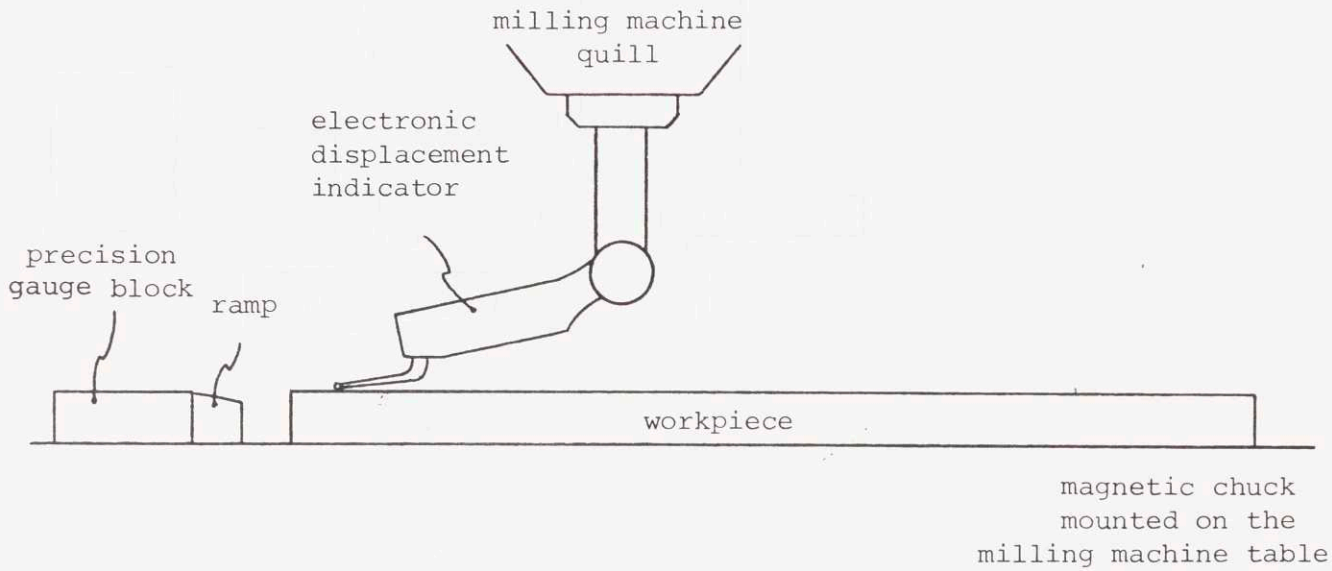

Figure 12. MRR Measurement Station

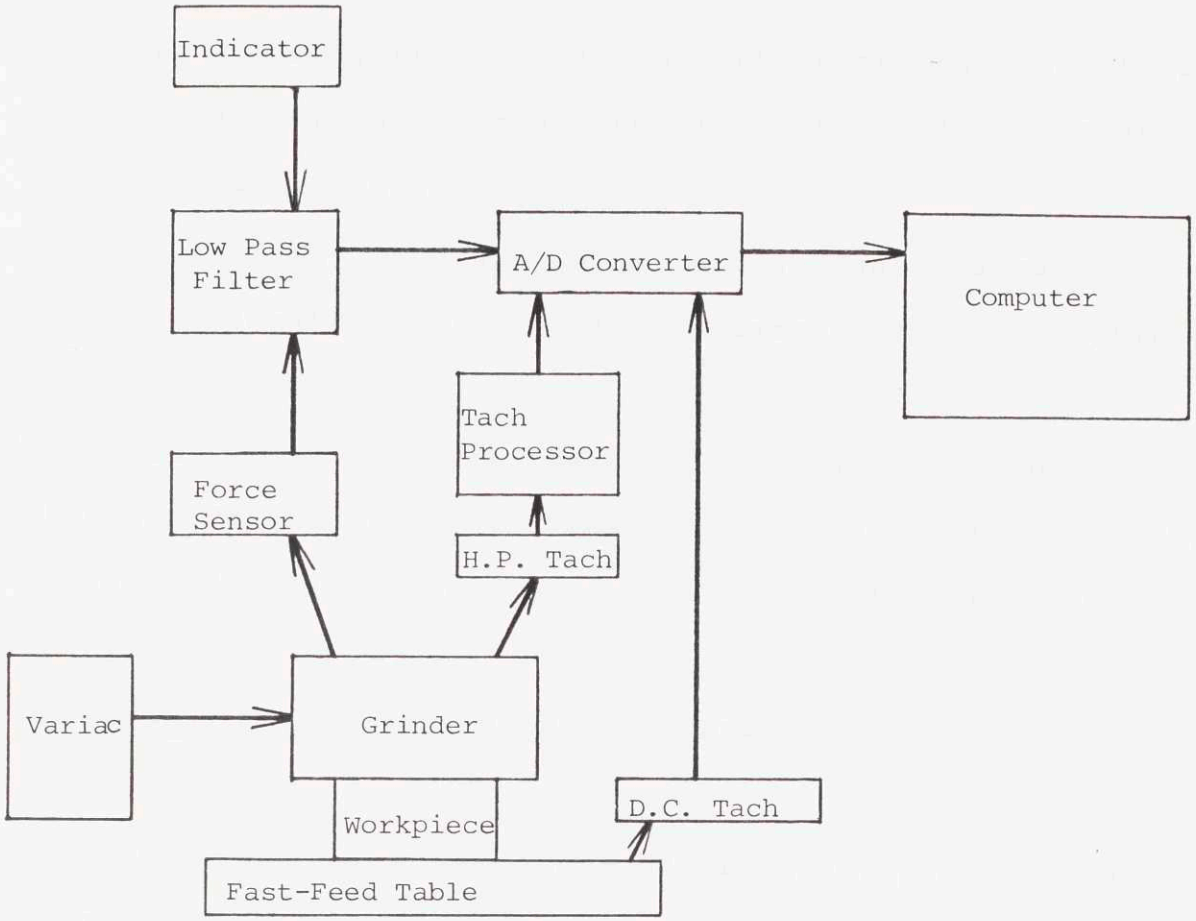

Figure 13. Revised data gathering system for quasi-steady state grinding. Not included is the Dektak II for measuring surface finish.

g. Quickly lower the workpiece after 8 1/4" has been ground.

h. For MRR, measure the new thickness down the middle and measure across the width in 15 places (every half inch).

i. For R_a, take 0.4" scans across the grooves (length-wise) centered on each of the 15 locations.

This procedure was repeated for four different feedspeeds and six grit sizes. Time constraints, however, permitted only four workpieces to be analyzed for MRR.

3. Procedure - increasing feed speed

A variation of the above quasi-steady procedure was conducted on two plates using a 36-grit disk. The purpose was to obtain data pertinent to the R_a model.

The sloped fixture was removed so that the normal force and depth of cut remained the same throughout the pass. Instead, the feed speed was slowly increased by turning a potentiometer in the table control box. With some practice it was possible to increase the feedspeed very smoothly.

IV. RESULTS

This chapter describes the results obtained from the experiments of the previous chapter. We start with perhaps the most striking result which is shown in Figure 14. On the right is a workpiece ground with a hand-held grinder. On the left is one ground with our experimental apparatus. The difference in R_a (which doesn't include the low-frequency waviness) is a factor of 2 to 3. Other experimentally ground pieces had surface finishes well below one micron, pushing the difference to a factor of 10. All of these were ground with 36-grit disks.

A. MRR Versus Π

The MRR-Π relationship in the first experiment was basically linear as shown in Figure 15. Recall that these data represent various normal forces (1.0 to 23N), feed speeds (1.1 to 15 in/min), disks (all 36 grit), and backings. A line was drawn to fit the data. From the line, K_1 and K_2 were evaluated as 8.4 J/mm^3 and 30 watts respectively.

The data for the 16 grit experiment is shown in Figure 16. One workpiece width was doubled as noted in the figure, yet there was no significant change in MRR or Π.

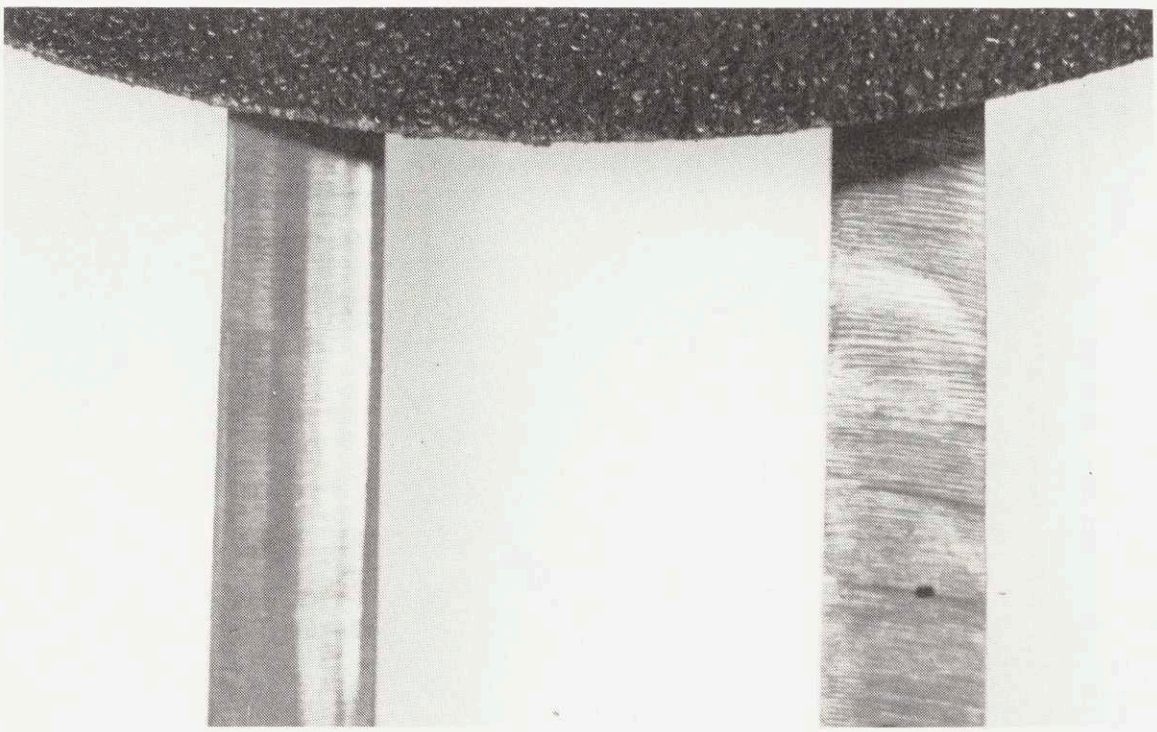

Figure 14. Experimental grinding on the left versus manual grinding on the right with a 36-grit disk.

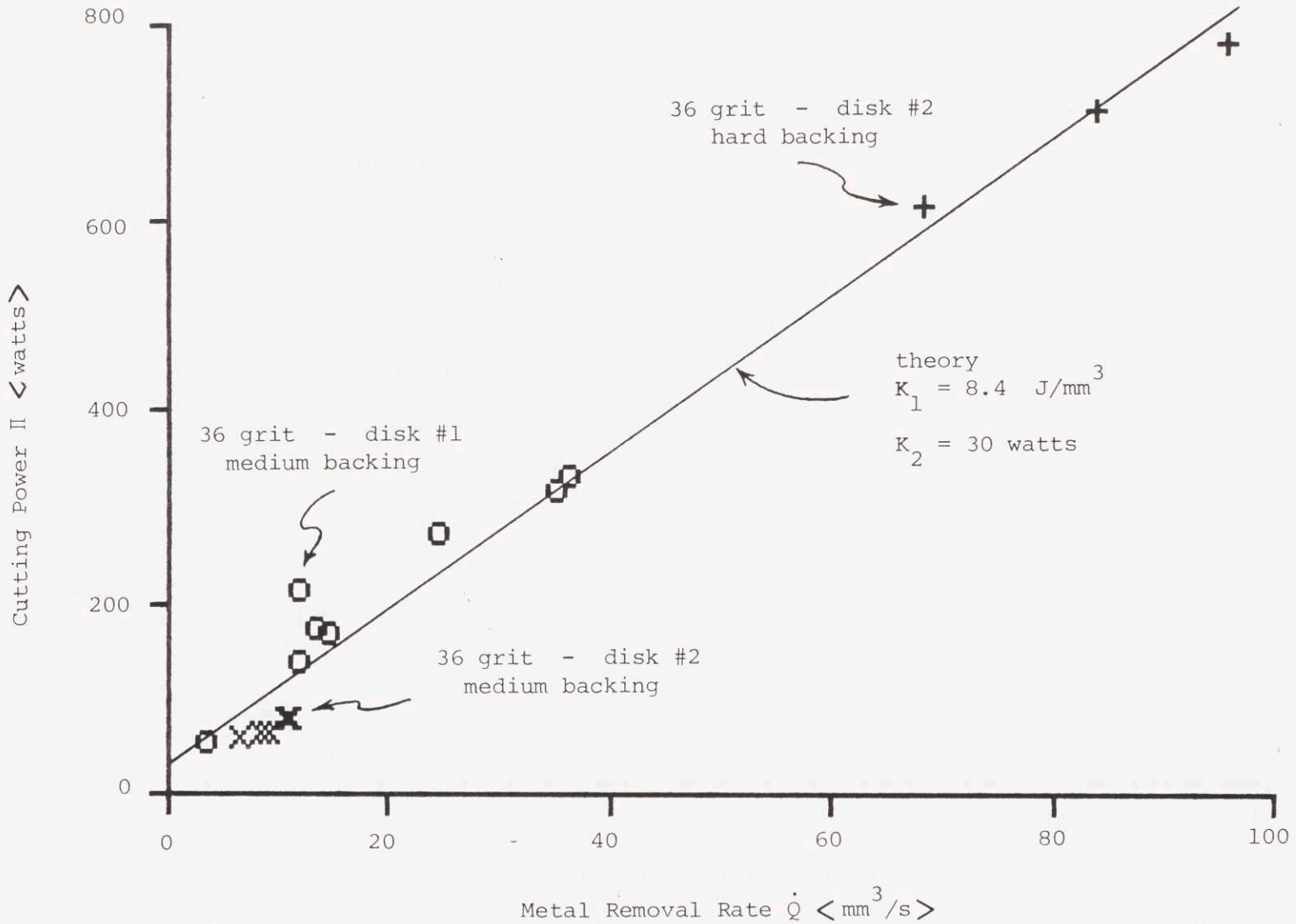

Figure 15. Π vs. MRR from the steady state experiment. Data is roughly linear although normal force, feed speed, disks (all 36 grit), and backing vary.

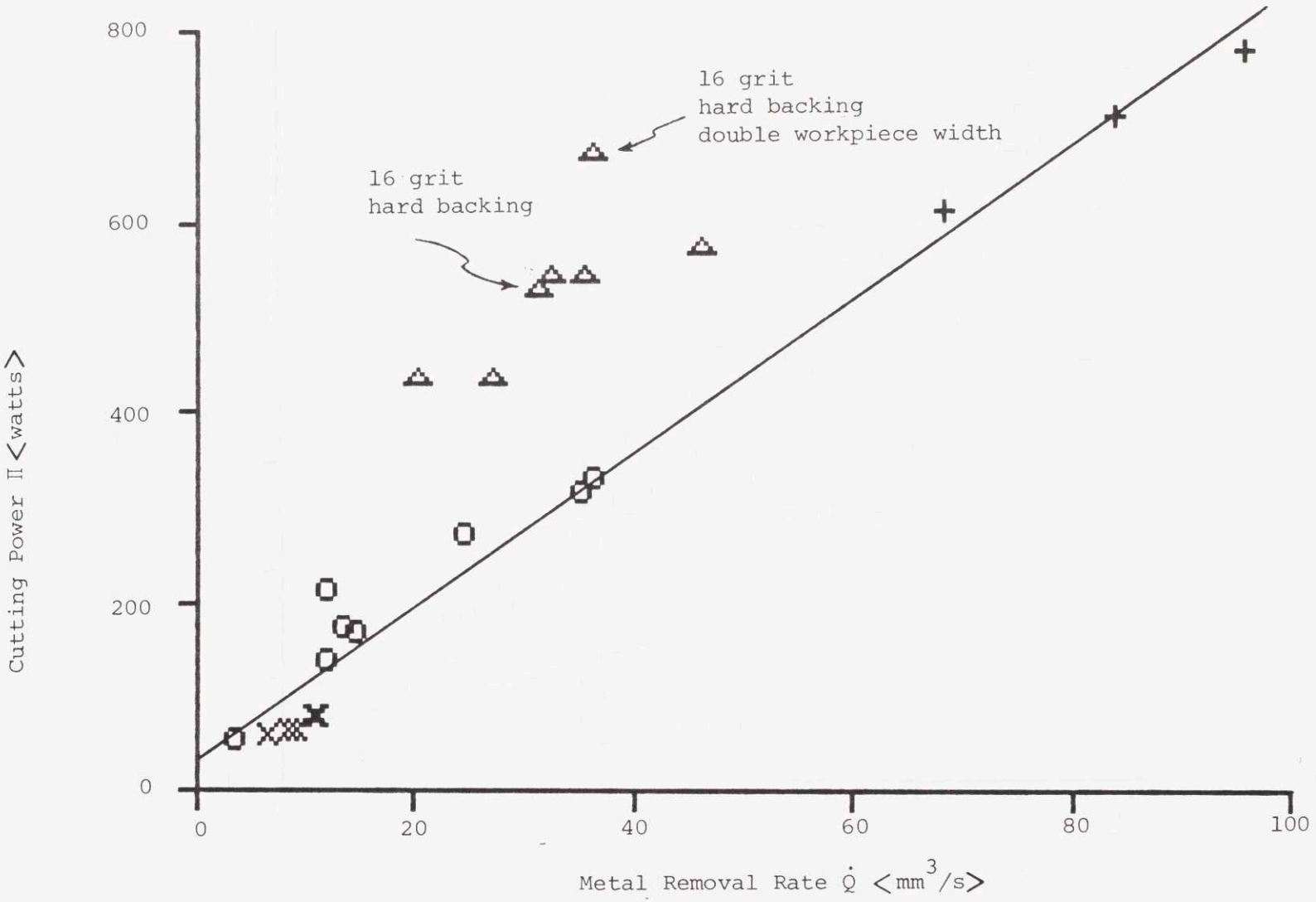

Figure 16. Steady state results including 16 grit data. This coarser disk requires more power for the same MRR. Note one workpiece was 1" wide instead of ½" wide with no significant difference in MRR or Π.

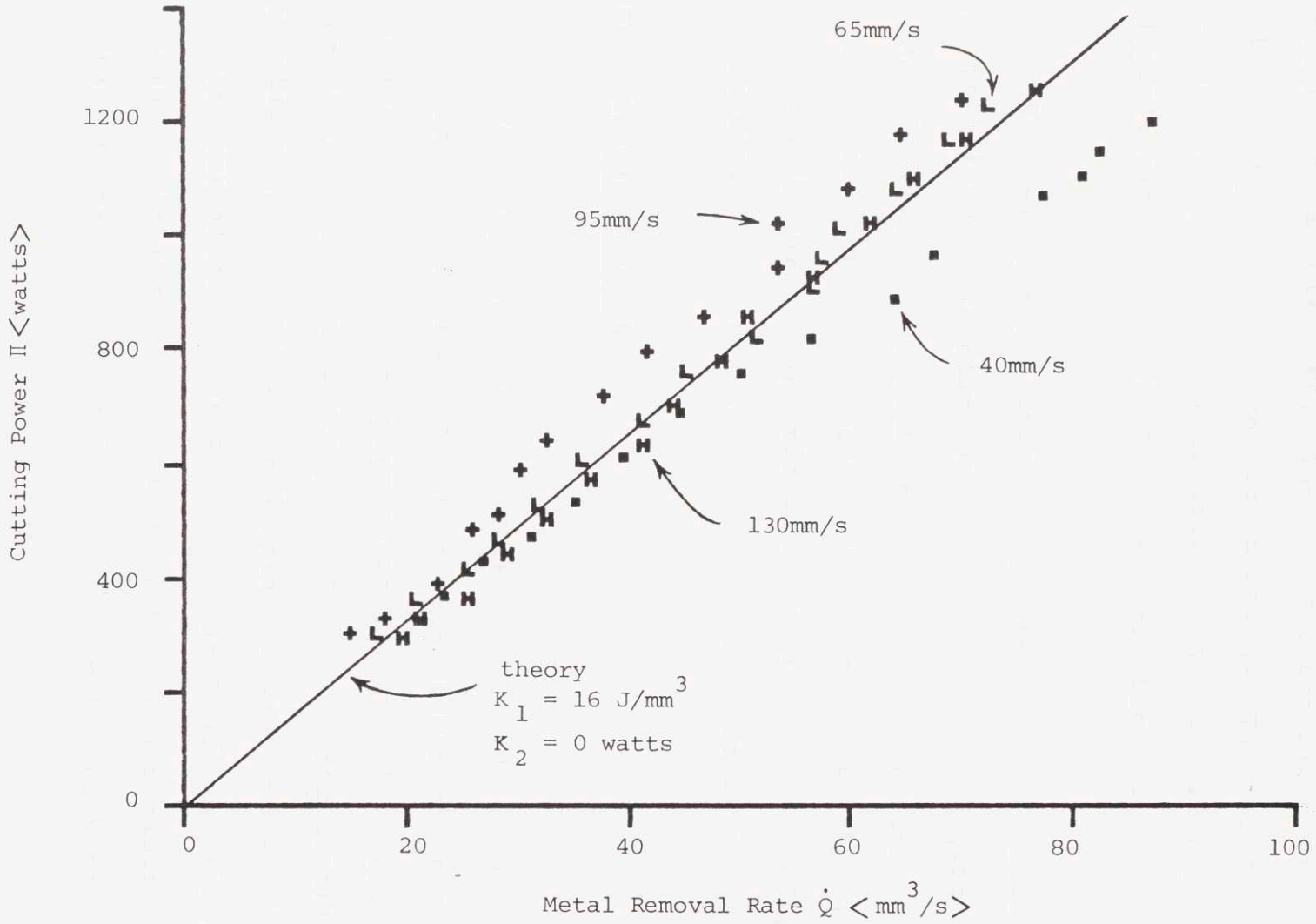

Figure 17. Π vs. MRR from quasi-steady state grinding with an 80-grit disk at 4 different feed speeds. Again, the relationship is linear with no significant dependence on feed speed.

It is somewhat surprising that this disk requires more power for the same MRR. The 16 grit anomalies will be discussed further in the next section. The important result, however, from this data is that the workpiece width doesn't seem to affect the MRR-Π relationship.

The relationship from the quasi-steady experiment with an 80-grit disk is also linear as plotted in Figure 18. Here, K_1 is about 15 (this finer-grit disk is designed to remove less metal for a given input power) and K_2 is essentially zero. The relationship seems to be independent of feedspeed, but more data is needed to confirm this.

B. Surface Finish

Table 2 presents the results of the grit parameter experiment. The values for γ are comparable to those found by other investigators using other methods.[8] However, the values for d and ℓ are probably low. From observations of plates ground at high feed rates, d and ℓ seemed to be two to four times larger than those in Table 2. Presumably the reason is that the different wheel speeds cause different inertial effects in the deflected backing.

Note that the parameter values for 16 grit-seem out of place. The 16-grit disks were different in more ways than just these parameters. The 16-grit disks had a significantly different composite coefficient of friction

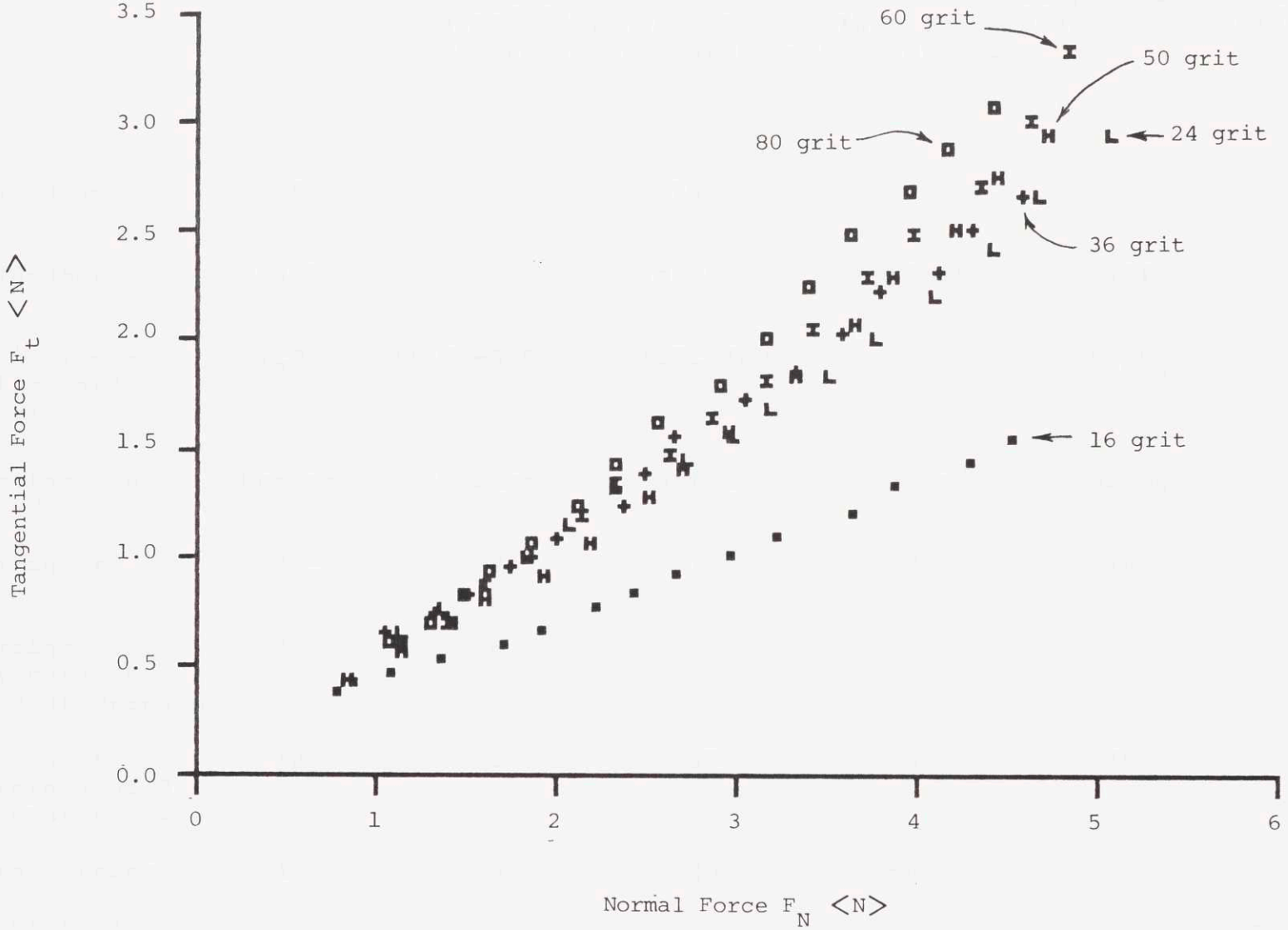

Figure 18. F_t vs. F_N for V_f = 40mm/s. The slope of each line is the respective μ_c.

Table 2. Results of the grit parameter experiment. The angle γ is the half-apex angle of an average grit, whereas d is the depth of penetration of that average grit. The base width of the average grit is $\ell = 2d\tan\gamma$.

Grit size	16	24	36	50	60	80
Tradename	Metalite	NorZon	NorZon	Metalite	Metalite	- - -
grit type - all closed coat	Al_2O_3	Al_2O_3-ZrO_3	Al_2O_3-ZrO_3	Al_2O_3	AL_2O_3	Al_2O_3
manufacturer	Norton	Norton	Norton	Norton	Norton	3M
Average γ	77°	67°	73°	78°	80°	77°
Average d <micron> of 7 largest grooves	8	16	9	6	6.6	4.3
Average ℓ <micron> of 7 largest grooves	70	75	59	56	75	37
Normal force <N> (approximate)	45	50	40	50	50	32

than the rest (see Figure 18) and exhibited **pull-out** at high wheel speed. My guess is that these disks are approaching their design limit for grit size.

Figure 19 shows the results of the steady state experiment in which only 36-grit disks were used. The theory curves were computed using the grit parameters in Table 2. Disk #1 was further along in wear than the disk #2, and as expected, R_a was lower.

Example surface profile traces are shown in Figure 20. Figure 20a shows where the traces were taken. In Figure 20b a family of grooves repeat over and over. If this surface were formed by only one grit (albeit strangely shaped), the pattern would be identically repeated with each revolution of the disk.

Notice also the great difference among the traces for different locations across the width of the workpiece. The grits tend to make deeper grooves when they first contact the workpiece. This is one reason for the scatter of data in Figure 19.

The results of increasing feed speed during the pass are shown in Figure 21 along with steady state results. The increasing force data was added to show the relative change in R_a due to normal force (also plotted in Figure 24). The dotted line is the same model as the solid line,

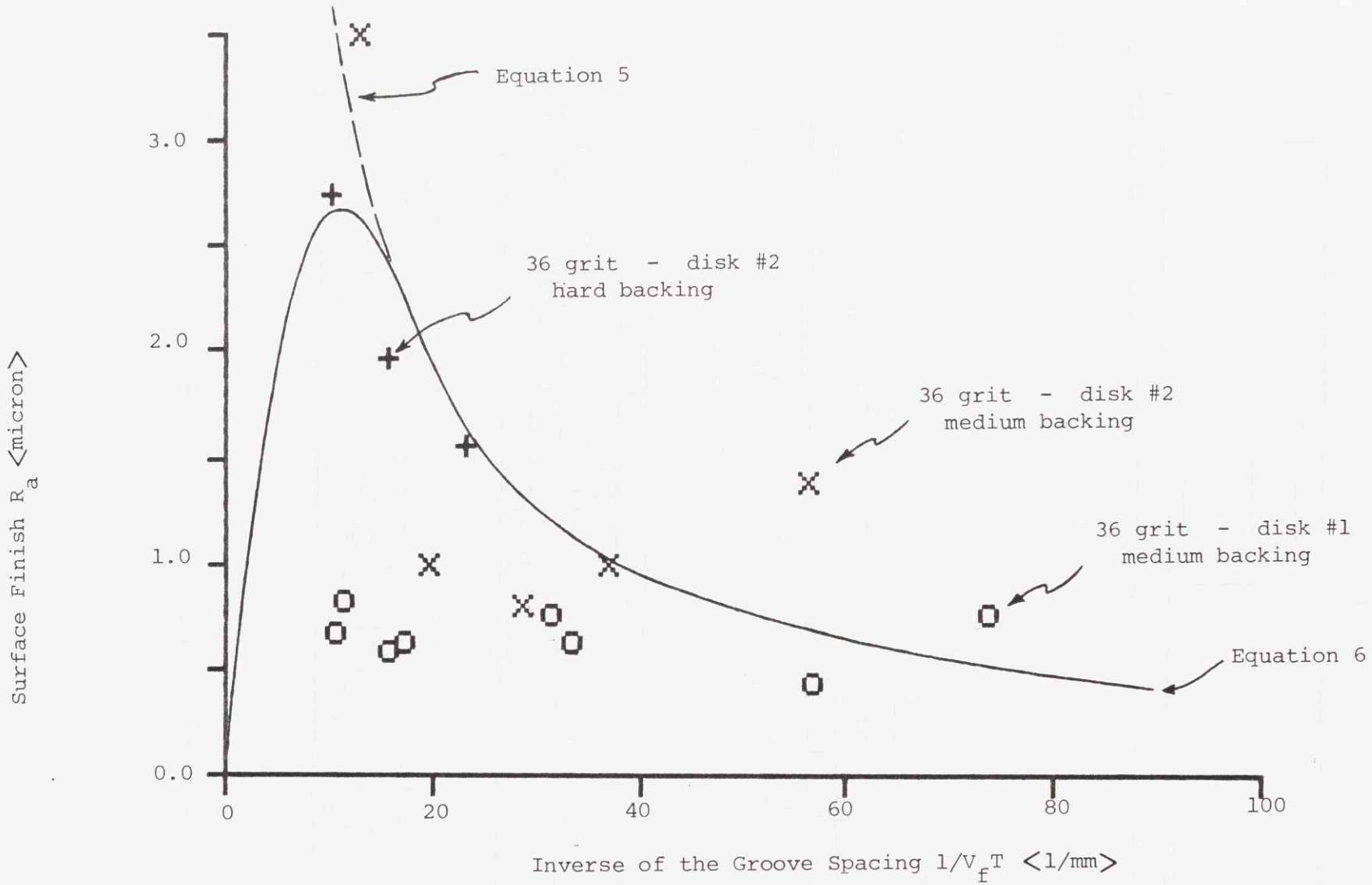

Figure 19. R_a model with data from steady state grinding.

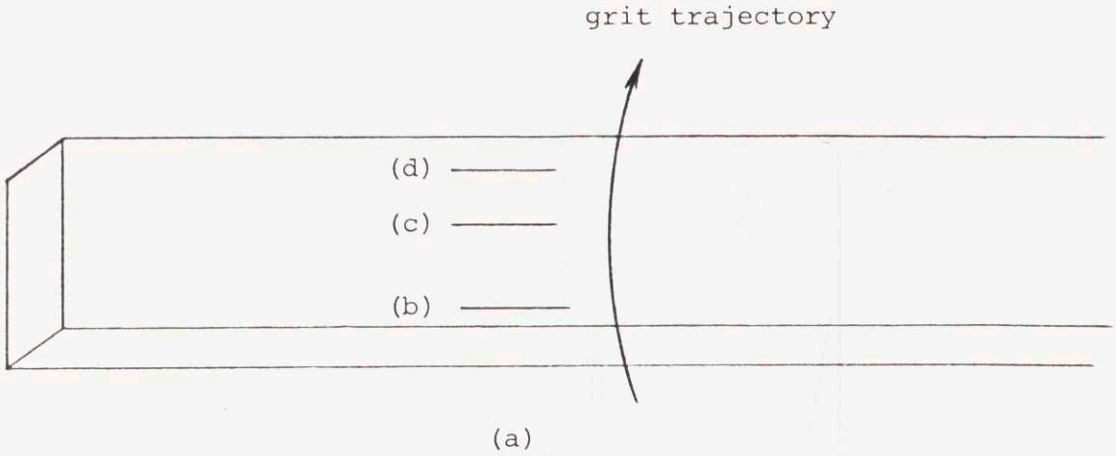

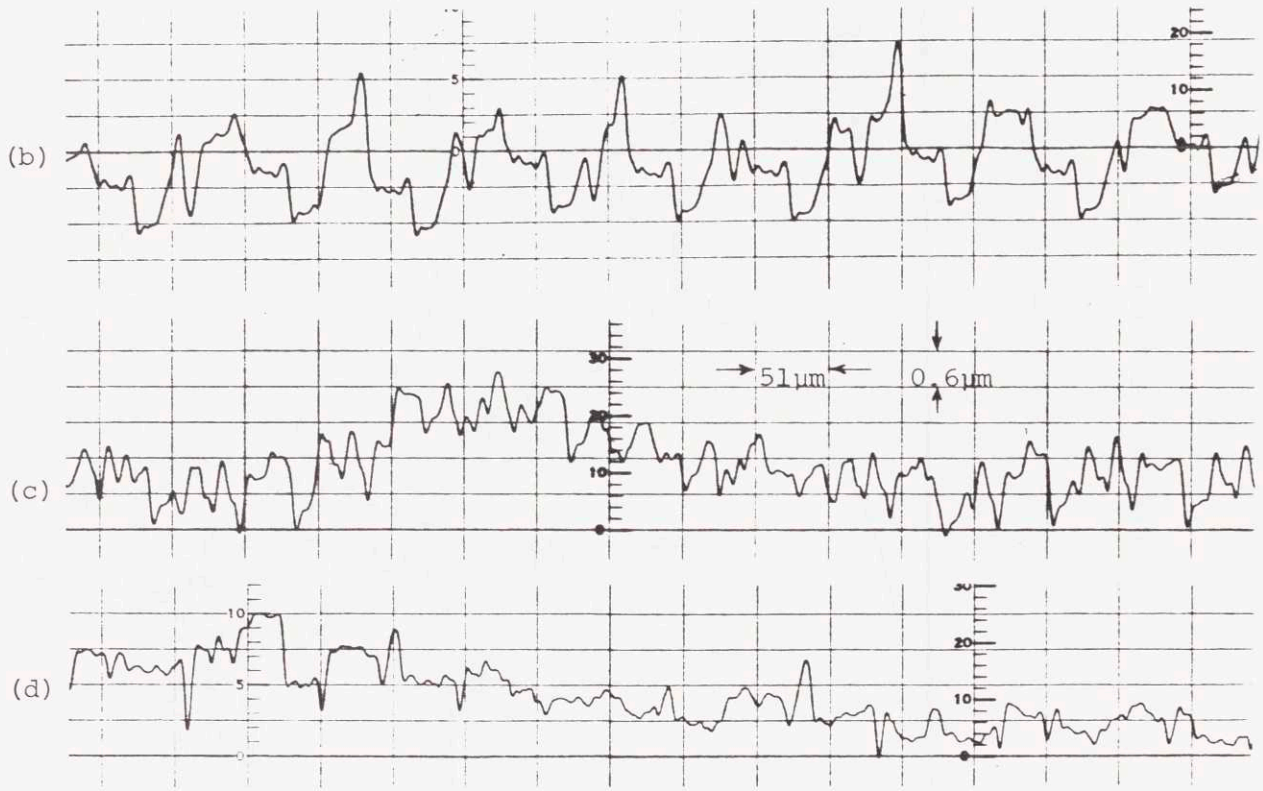

Figure 20. Surface finish at three locations on the workpiece

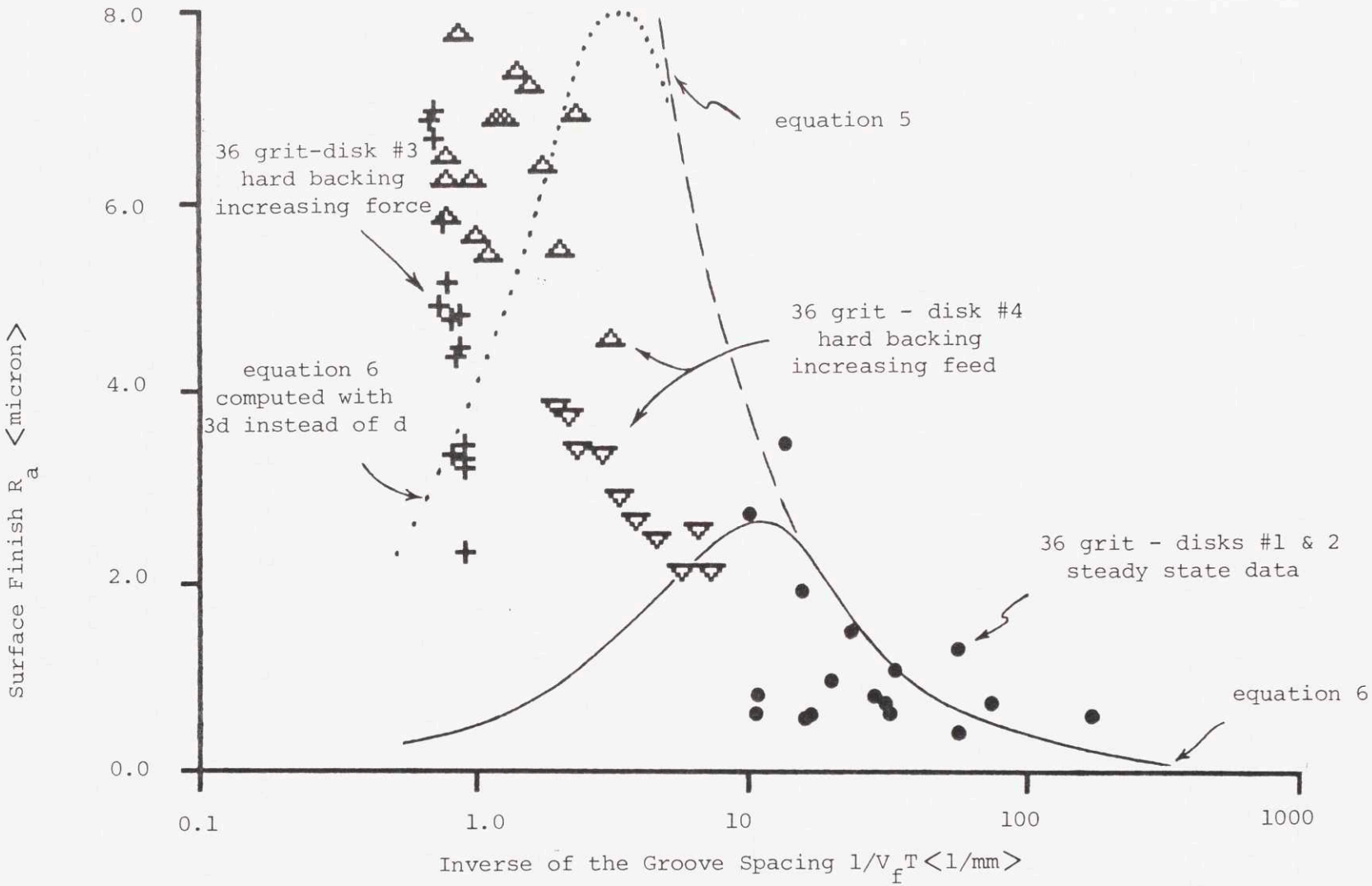

Figure 21. Combined surface finish results

but d was replaced with 3d.

As expected, the model is not accurate for small $1/V_fT$. The data for small $1/V_fT$ has a spread from 2 to 8μm. As $1/V_fT$ increases, the data gets sandwiched under the equation 5 curve.

The next three figures are the results of the sloped experiment. In Figure 22, surface finish is plotted versus normal force for the 24 grit size at four feed speeds. Likewise, Figure 23 is for the 60 grit size. The rest of the grit sizes had less correlation between R_a and F_N. Figure 24 is a graph of all six grit sizes at the lowest feed speed.

Recall from Chapter II that d is expected to be a monotonic function of normal force and that if d increases, then R_a increases. Therefore we should expect R_a to increase monotonically with normal force. Why, then, the discrepancy?

The normal force in figures 20-22 is the composite normal force at the contact patch, whereas the normal force referred to in the model is the normal force on the grit which determines R_a. These forces are not the same. In fact, I have seen the perimeter of the disk lose contact with the workpiece, under the extreme conditions of a large normal force and a soft backing.

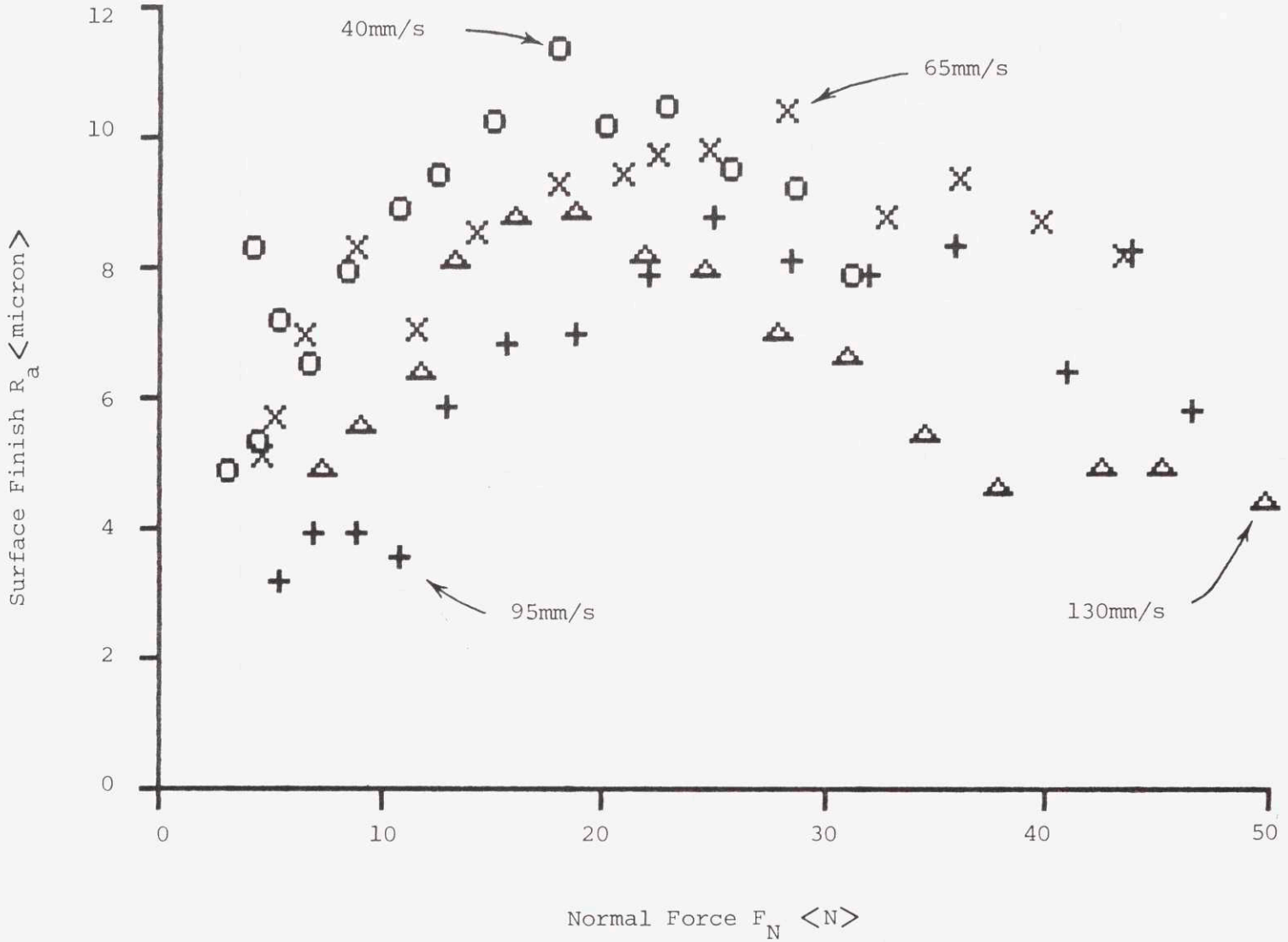

Figure 22. R_a vs. F_N from quasi-steady grinding with a 24-grit disk. R_a increases with F_N as one might expect, but eventually decreases.

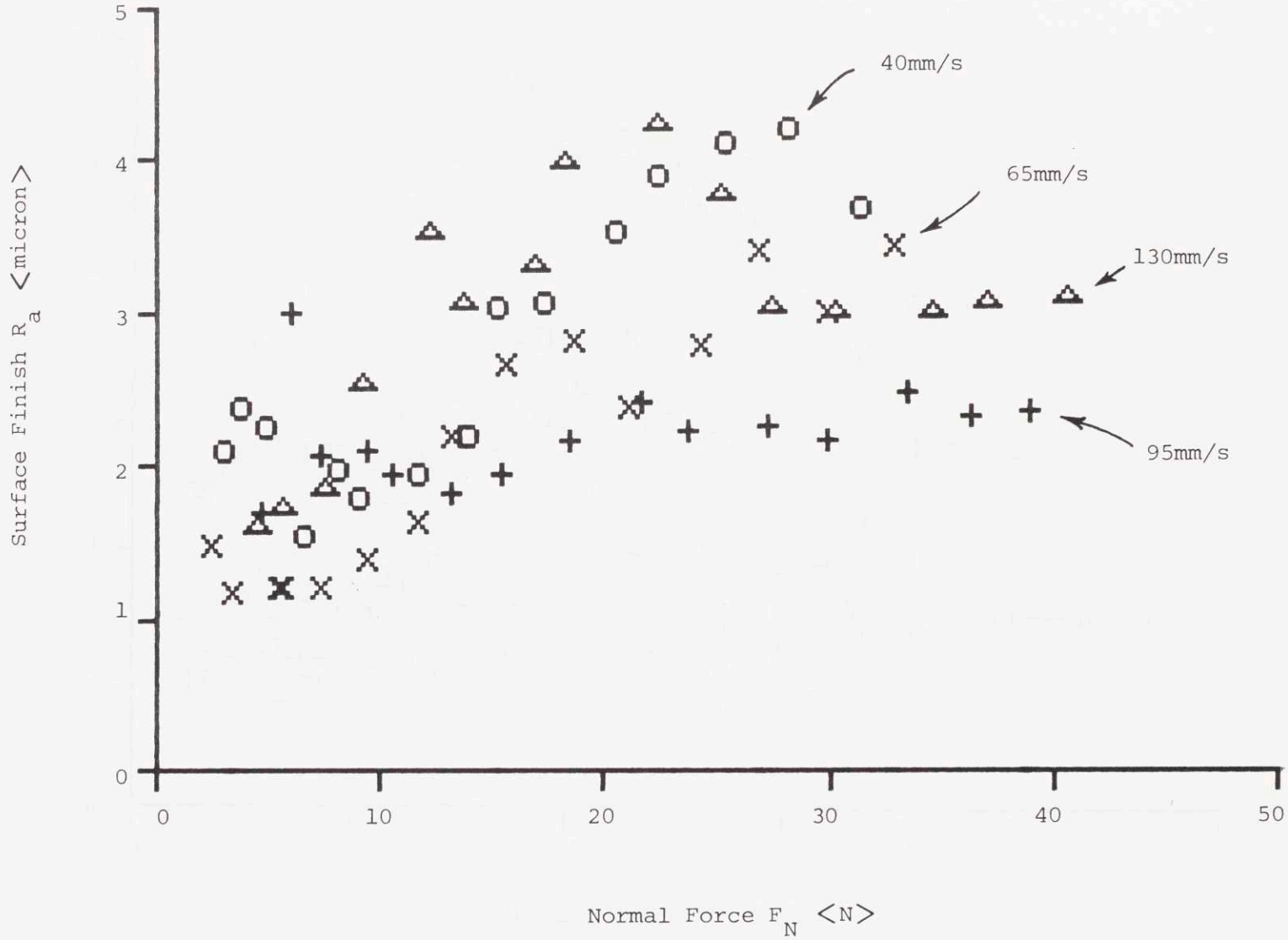

Figure 23. R_a vs. F_N for 60 grit

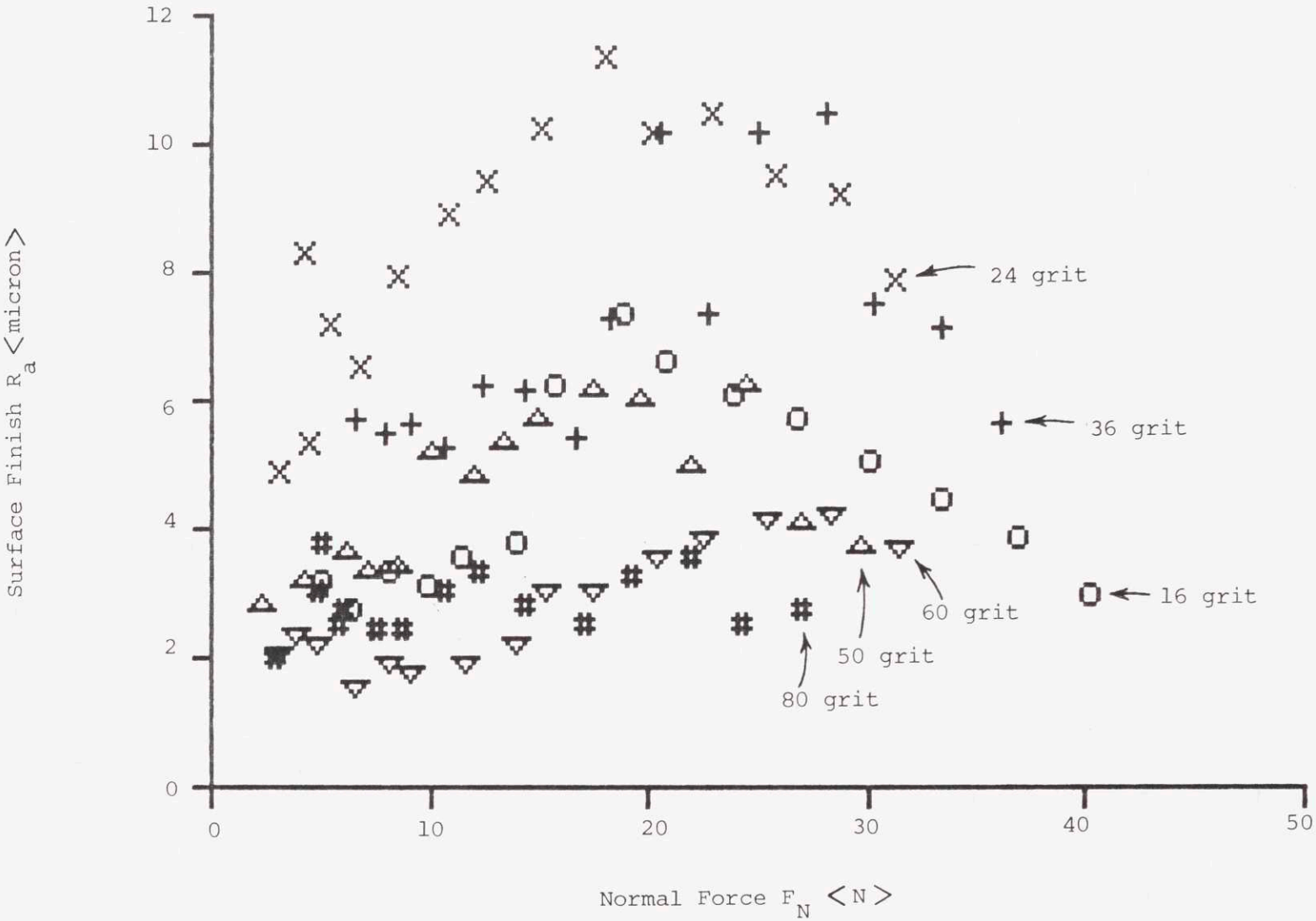

Figure 24. R_a vs. F_N at V_f = 40mm/s. Generally the R_a dependence on F_N increases with grit size.

V. DISCUSSION

A. MRR

We now see that $\dot{Q} = C_o + C_1 \Pi$ is a valid relationship and that C_o and C_1 do not depend significantly on V_f, F_N, or bead width. Thus the equation is an adequate model of instantaneous MRR for our purpose (according to section II.A). The following describes how C_o and C_1 could be tracked.

The vision system mentioned in Chapter I will measure the change in cross-sectional area of the bead (due to a grinding pass) at many positions along the bead. This change in area multiplied by the feed speed that the grinder had at that point is the MRR at that point. With the measured Π at that point in the pass, we have an estimate of C_1 which is approxmiately $\dot{Q}/\Pi$ for $C_0 \approx 0$.

If this data is recorded for all measured points along the pass, a line will emerge in the $\dot{Q}$ - Π plane. A least squares fit to the data would give C_o and C_1. This information could be used to plan the next pass and so on.

If the system remembers C_1 over many passes, then wear could be detected and, at the appropriate time, (according to some economic criteria), the disk could be discarded.

B. Surface Finish

R_a has been modelled approximately. The model indicates that R_a improves as ω $(=2\pi/T)$ increases and V_f decreases. Both of these changes have their limits unfortunately. F_N also has some effect on R_a, but this has not been modelled yet.

The upper limit of ω is due to the centrifugal force on a grit which is proportinal to $\omega^2 R$. The limit of the centrifugal force is that which causes **pull-out** .

A limiting factor for low V_f is the maximum allowable temperature of the workpiece. The temperature rise is iversely proportional to V_f. Other parameters can be changed to push back the limit of V_f; Π and p can be lowered. A cooling fluid might also be used. The other lower limit of V_f is the time constraint of production.

C. Process Planning

What practical application does all this have? The auto manufacturers want to know: How many stations (how many grit sizes) will be needed to remove the bead, leaving an acceptable finish within the production cycle time t_c? This question is important because large robots are expensive. Although the results of this thesis don't give

the answer, I envision a two-station system which is described in the remainder of this section.

Using a coarse-grit disk, such as 24, the first station would remove most of the weld bead very quickly (very high MRR). Then on this station's last pass, in order to obtain the best R_a, V_fT and F_N would be as low as possible according to the constraints listed below.

With a fine-grit disk, perhaps as fine as 240, the second station would lower the final surface finish even further, removing any stray chips that sometimes remain attached to the surface. This station would produce a random scratch pattern on its last pass. (We have been told that a random scratch pattern is not as visible after the car has been painted as a uniform scratch pattern of the same R_a value.) One method of obtaining random scratches is to maneuver the robot in some non-uniform motion while a hub-less disk spins very slowly with $\theta=0$ - similar to a floor buffer. The other way is to use a grinder which is specially designed to produce non-uniform scratches.

Force control will likely suffice for the second station, since MRR will be **extremely** low. The first station, on the other hand will require several levels of sophisticated control.(7) The following constraints apply to the first station.

(a) The bead of volume V_b must be removed within the cycle time t_c.

$$V_b = \int_0^{t_c} \dot{Q}(t)dt$$

where $\dot{Q}(t)$ is the actual MRR as a function of time. Note that $\dot{Q}(t) = 0$ between passes. This constraint provides a lower limit on the average MRR.

(b) There is a lower limit on feed speed V_f depending on the number of passes n, the cycle time t_c, and the length of the bead b.

$$\frac{1}{nb}\int_0^{t_c} V_f(t)dt + \frac{1}{(n-1)t_o} \geq \frac{1}{t_c}$$

where t_o is the non-grinding time for each pass (assumed independent of V_f).

(c) The surface finish produced by the first station must be smooth enough that the second, fine-grit station can finish it. "Smooth enough" is denoted R_a^* in the following constraint for the

last pass of the first station:

$$R_a = fn(V_f, \quad T = \frac{2\pi}{\omega}, \quad F_N = \mu F_t) < R_a^*$$

The function fn has been partially modelled by equations 5 and 6.

(d) The temperature of the workpiece T_w must not be higher than some critical temperature T_{cr} at any time during the process.

$$T_w < T_{cr}$$

T_w must be modelled further, meanwhile some upper bound is assumed to exist for

$$\Delta T \approx \Pi \sqrt{\frac{p}{V_f}}$$

which decreases with successive grinding because the workpiece generally gets hotter with each pass. Of course, this constraint will not be as restrictive if a cutting fluid is used.

(e) The force on each grit must be less than that which causes **pull-out** F_p. The force on each grit is composed of the tangential force F_t and the centrifugal force. The following is an approximate equation:

$$\frac{1}{gA_p} F_t + m\omega^2 R_c < F_p$$

A_p - area of contact patch

g - number of grits cutting

m - mass of the average cutting grit

This normally would not be a consideration in manual grinding, but it may be important in the automated system.

(f) For our grinding geometry, a limit exists on the normal force due to the deflection of the disk and backing, which is illustrated in Figure 25. The constraint here is that the disk not touch the parent surface!

$$h > \delta = fn(F_N, \theta, \text{disk \& backing properties})$$

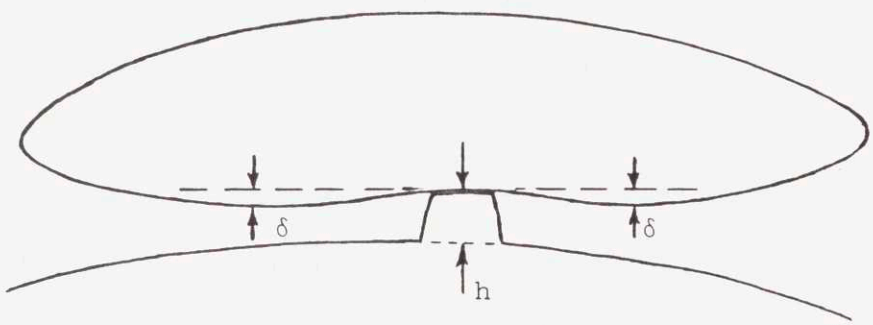

Figure 25. Deflection of the disk under a high normal force.

If this turns out to be important, the backing could be redesigned. However, force control of grinding would be more difficult with stiffer backings.

If the first station is able to meet constraints a through f, then the 2-station system is feasible.

How can these constraints be used to plan passes? As mentioned before, R_a is not of concern until the last pass. For the best R_a on the last pass, V_f should be as low as possible on the last pass, which implies that MRR be as high as possible before the last pass.

For high MRR, Π must be high which will be limited by constraint f, e, or a combination of d and b. For a given system, one of these will be the limiting factor. Constraint d alone cannot limit Π, beause V_f can be increased to as high as the robot's top speed. On the other hand, because of constraint b, there is a diminishing return from higher feed rates, because more passes are needed - which increases the non-grinding time. In other words, the instantaneous $\dot{Q}$ may be high, while the average $\dot{Q}$ over several passes may be low.

Constraint e will limit both F_t and ω. (Recall that $\Pi = \left|F_t \omega R_c\right|$.)

If a flexible backing is used, then constraint f will also apply. (Recall that $F_t = \mu_c F_N$.) Since h decreases, Π - thus MRR also - must decrease with each pass. Constraint d may also imply this decrease in Π and MRR.

The remaining cross-section area A_r constrains $\dot{Q}/V_f$. This is a variation on constraint a. Note that this is not an upper or lower bound, but a prescribed quantity:

$$A_r = \dot{Q}/V_f \approx C_1 \Pi/V_f = C_1 F_t \omega R_c/V_f \qquad (7)$$

From constraint b we must have that

$$\frac{1}{b} \int_0^{t_r} V_f(t)dt \geq \frac{1}{t_r}$$

on the last pass where t_r is the time remaining in the production cycle. The other constraints are c and d. For R_a's sake, we want low V_f, which is limited by

$$\Delta T \approx \Pi \sqrt{\frac{p}{V_f}} = \frac{A_r}{C_1} \sqrt{pV_f}.$$

(p can't be changed very much.) Now V_f is bounded, which also bounds Π (from equation 7), but R_a can still be improved. F_t can be decreased while ω is increased proportionately. Both of these changes tend to improve R_a.

Again, but more specifically, if this R_a can be made less than R_a^*, then this envisioned grinding system is feasible.

VI. CONCLUSIONS

This chapter is a summary of major findings already discussed in the Results and Discussion chapters:

1. MRR is linear with cutting power: $Q = C_o + C_1 \Pi$

2. The coefficients of the above linear equation are, at worst, not strongly dependent on the feed speed, normal force, or bead width.

3. R_a improves as much as a factor of 10 with decreasing feed speed and increasing wheel speed. R_a depends on F_N also, but this has not been modelled yet.

4. Equation 5 is an upper estimate for $V_fT > \ell$ and simply an estimate for $V_fT < \ell$.

5. The above conclusions, along with other constraints on the system can be used by the system to plan future passes. Generally speaking, high MRR is desirable in the first few passes, decreasing with later passes, and low V_fT is needed on the last pass to produce the best finish.

VII. RECOMMENDATIONS

1. More data is needed to determine the validity of the models presented here. Other parameters besides F_N, V_f, disks, and bead width should be changed to see if the MRR or R_a are affected. Try different orientations, stiffer backings, and perhaps a cooling fluid.

2. The R_a model should be updated to include the normal force.

3. Wear needs to be investigated in terms of the models. Are the MRR and R_a equations valid as the disk wears, provided that the coefficients are updated? When is the best time to change to a new disk?

4. Non-steady state grinding should be investigated because the system must be able to start and end the pass, grind around corners, and remove lumps.

5. A model for the workpiece temperature should be developed and verified with data.

REFERENCES

1. Namba, Y., Tsuwa, H., "Monte Carlo Simulation of Belt Grinding Process," Annals of the CIRP, Vol. 25, No. 1, 1976, pp. 241-246.

2. Wright, K.L., "Performance of Coated Abrasives," M.S. Thesis, MIT Department of Mechanical Engineering, January 1985.

3. Shibata, J., "The Relation Between the Wear of Grain Cutting Edges and Their Metal Removal Ability in Coated Abrasive Belt Grinding," Wear, Vol. 55, 1979, pp. 331-334.

4. Kenwood, G., "Process Modelling of Weld Bead Grinding as Part of a Robotic Solution," M.S. Thesis, MIT Department of Mechanical Engineering, 1984.

5. Shaw, M.C., "How to Estimate Grinding Forces and Power," Machinery, March 1968, pp. 85-87.

6. "Automation of the Auto Body Solder Filler Grinding Operation, Final Report," Charles Stark Draper Laboratory, Inc., December 1982.

7. Nevins, J., Whitney, D., et al, "Adaptive Control, Learning and Cost Effective Sensor Systems for Robotics or Advanced Automation Systems," First Annual Report, Charles Stark Draper Laboratory, Inc., 1984, pp. 50-58.

8. Phadke, M., Wu, S., Burney, F., "Evaluation of Coated Abrasive Grain Geometry and Wear via Continuous Time Series Models," Wear, Vol. 31, No. 1, Jan 1975, pp. 29-38.

Appendix A - Orientation

Three orthogonal angles of orientation of the disk with respect to the workpiece are possible input parameters of the process. That is, the angles may affect one or more of the five output parameters. Although understanding their effect on the process is not the main thrust of this study, the angles are discussed here for completeness.

The angle between the feed speed (V_f) direction - assuming a unidirectional feed - and the grit velocity (V_g) direction is called the orientation angle Ψ in Figure 26. V_g is the product of wheel speed ω and the radius to the center of the contact patch R_c. The orientation angle will affect the scratch pattern on the surface and the surface finish R_a. In this thesis Ψ is approximately 90°.

As shown in Figure 26, the angle of inclination θ is the angle of rotation about the V_g axis measured from a tangent to the workpiece near the contact patch. In general θ is inversely proportional to the contact patch size for a given normal force. This fact was demonstrated in an early test. Typically in the manual operation, θ varies from 0 to 20°. For the experiments described in this paper, θ is a constant 20 degrees.

The tilt angle τ, as shown in Figure 26, is a rotation orthogonal to θ. This parameter turned out to be important for efficient snagging.(4) On a flat surface τ is always zero. If the disk is tilted when grinding a flat surface, the contact patch moves around the disk accordingly and the direction of V_g - which is the reference direction - changes. Throughout the experiments τ is a constant equal to zero.

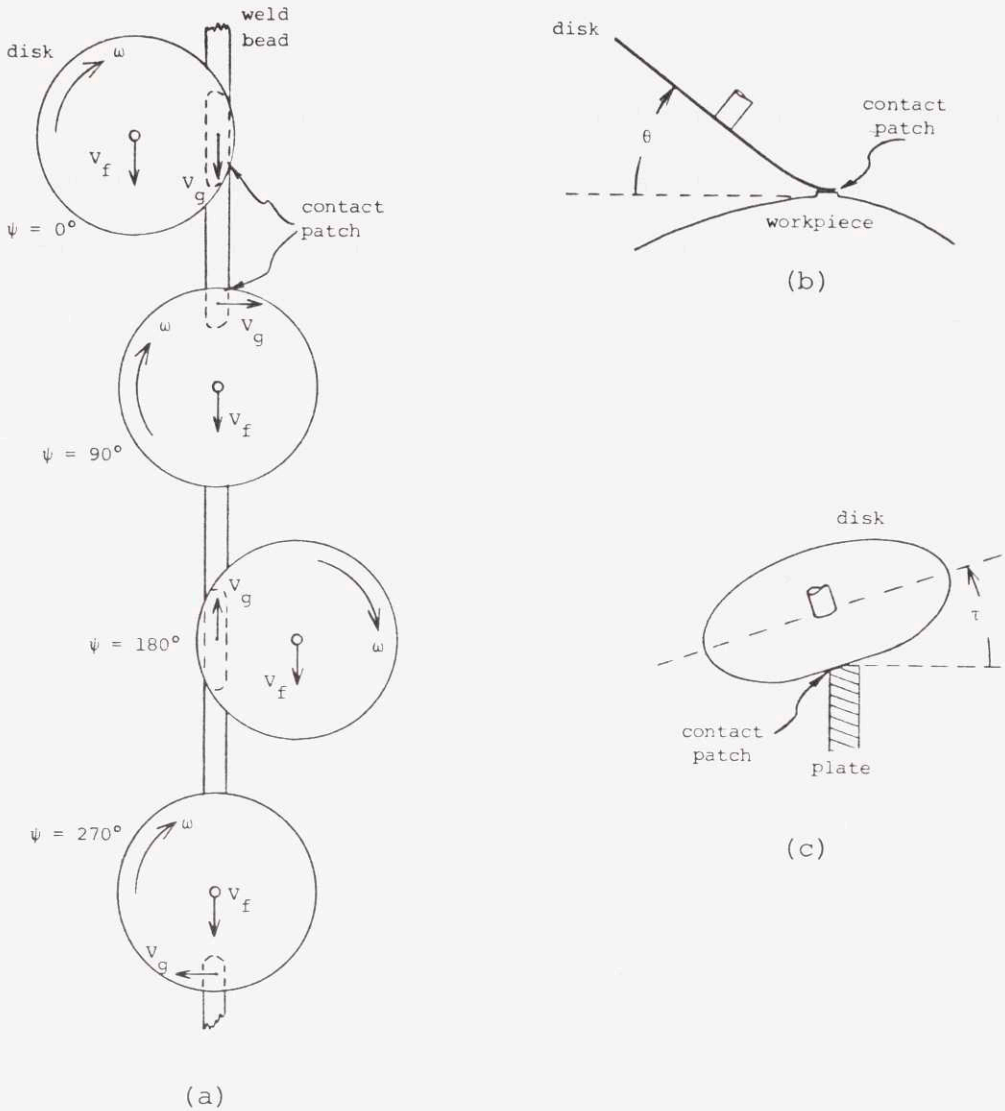

Figure 26. Orientation Angles. (a) Schematic of ψ at four different values. Arrows show direction of velocity only - not relative magnitude. (b) Schematic of θ (exaggerated) at $\psi = 0°$. (c) Schematic of τ in edge grinding of a thick plate.

Appendix B

This appendix lists the coordinate transformations used to compute forces at the contact patch. The geometry of the apparatus including cordinate systems is shown in Figure 27. The force sensor measures support forces in coordinate system x-y-z which are translated by the following equations into coordinate system 1-2-3 (whcih is not rotating with the disk).

$$F_1 = F_x\cos\beta - F_y\sin\beta$$

$$F_2 = F_y\cos\beta + F_x\sin\beta$$

$$F_3 = F_z$$

$$M_1 = M_x\cos\beta - M_y\sin\beta - D_3F_2$$

$$M_2 = M_y\cos\beta + M_x\sin\beta + D_3F_1 - D_1F_z$$

$$M_3 = M_z + D_1F_2$$

F represents the force in the subscripted direction, and M represents the moment likewise. D_1, D_3, and β are displacements and rotation between the two coordinate frames

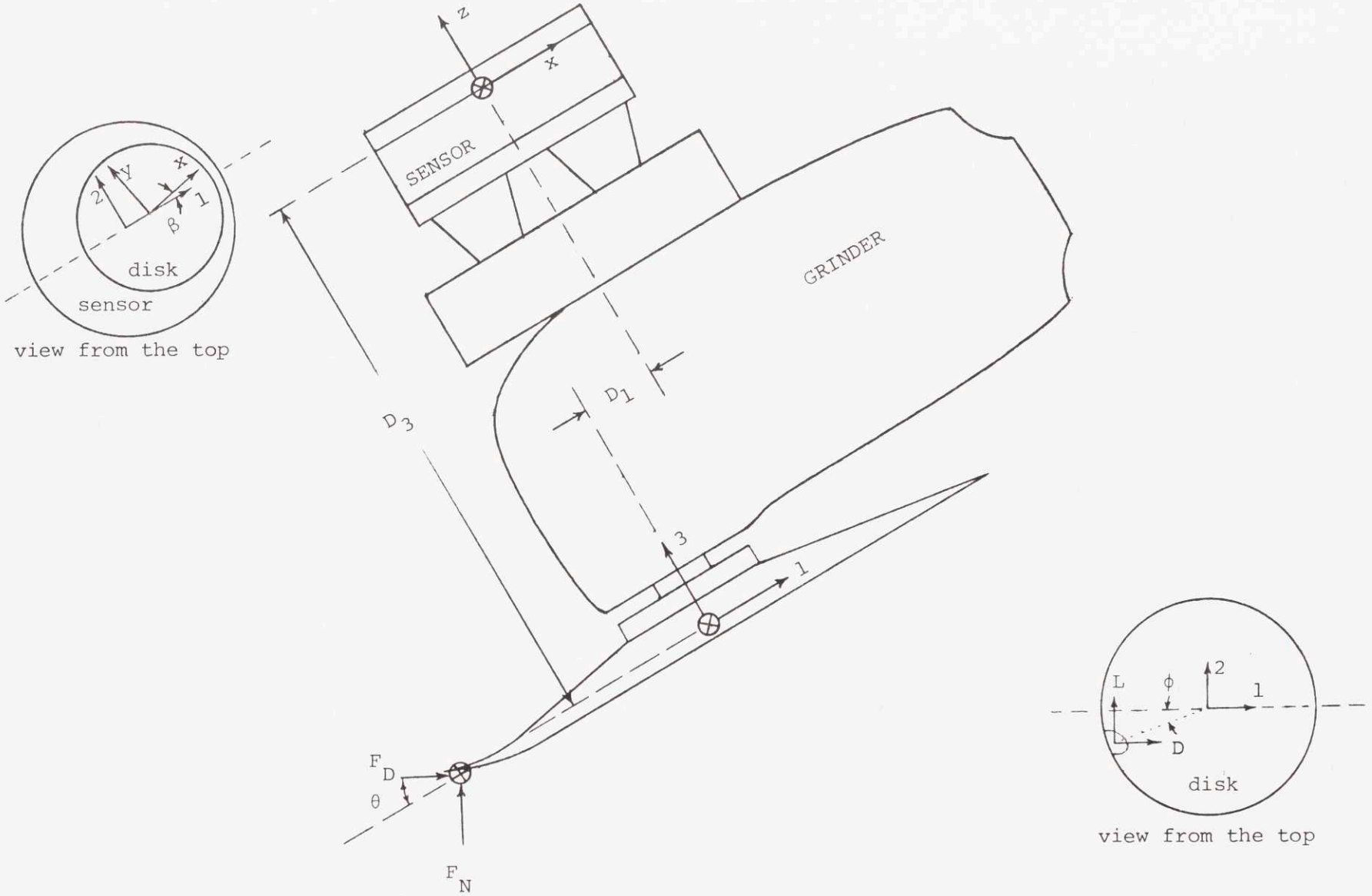

Figure 27. Schematic of coordinate systems. The sensor measures 3 forces and 3 moments in the x-y-z system.

as shown in the figure. Note that D_1 is essentially a constant except for some very small displacement at the shock mounts, but D_3 depends on the deflection of the disk as well as the deflection of the shock mounts. In this thesis, D_3 is assumed a constant average displacement - incurring a maximum error of 1%.

The second translation is from the center of the disk to the contact patch. The patch coordinate system is represented by D(drag), L(lateral), and N(normal) directions in the following equations.

$$F_D = F_1\cos\theta - F_3\sin\theta$$

$$F_L = F_2$$

$$F_N = F_3\cos\theta + F_1\sin\theta$$

$$M_D = M_1\cos\theta - M_3\sin\theta + F_N R\sin\phi - F_2 R\cos\phi\sin\theta$$

$$M_L = M_2 - F_3 R\cos\phi$$

$$M_N = M_3\cos\theta + M_1\sin\theta + F_L R\cos\phi\cos\theta - F_D R\sin\phi$$

The origins of D-L-N can be defined in such a way that M_D and M_L are zero. If the origin is located at the centroid of the force distribution in the Normal direction, then by definition of centroid, M_D and M_L are zero. We can now solve for two other variables, for example, R and θ as shown below.

$$F_D = F_1\cos\theta - F_3\sin\theta$$

$$F_L = F_2$$

$$F_N = F_3\cos\theta + F_1\sin\theta$$

$$\phi = \tan^{-1}[(M_3\sin\theta - M_1\cos\theta)F_3/F_N M_2 + F_2\sin\theta/F_N]$$

$$R = M_2/F_3\cos\phi$$

$$M_N = M_3\cos\theta + M_1\sin\theta + F_L R\cos\phi\cos\theta - F_D R\sin\phi$$

In this thesis only the first three equations were used. The tangential force is the resultant of F_D and F_L:

$$F_t = \sqrt{F_D^2 + F_L^2}$$

Appendix C

This appendix details some of the components of the measurement system.

1. Steel force sensor

This 6-axis strain gauge sensor was designed and built here at Draper. The sensor was calibrated on a 2-axis rotary table by loading the sensor in different orientations with weights. More than 6 configurations were used so that a least squares fit to the data could be obtained with a pseudo-inverse matrix opration.

The calibrated sensor had the following characteristics:

- overall accuracy of F_z: within 10%
  of others: within 5%
- cross-coupling between axes: 3%
- sensitive to temperature changes
- internal noise levels after filtering:

F_z $\pm$ 2N

F_x & F_y $\pm$ 1/2N

moments $\pm$ 1/3N

Sensor drift due to temperature changes was alleviated by allowing a warm-up period and biasing the sensor with the disk spinning just prior to each grinding pass. The calibration was periodically checked for accuracy.

2. High precision tachometer

The tachometer uses an optical limit switch to detect the period of rotation of the disk. By integrating while the switch is closed, the circuit produces a voltage proportional to the period of the disk.

The tack was calibrated by measuring the period of the limit switch output on an oscilloscope. The calibrated accuracy was $\pm$ 1Hz or about 1 to 2%.

3. Fast feed table and d.c. tachometer

The fast feed table was equipped with a $\pm$ 3 volt d.c. tach which had plenty of resolution for our purposes.

The fast feed table was controlled open loop. In quasi-steady grinding the feed speed was fairly constant throughout the pass, although the normal force increased an order of magnitude as shown in Figure 28.

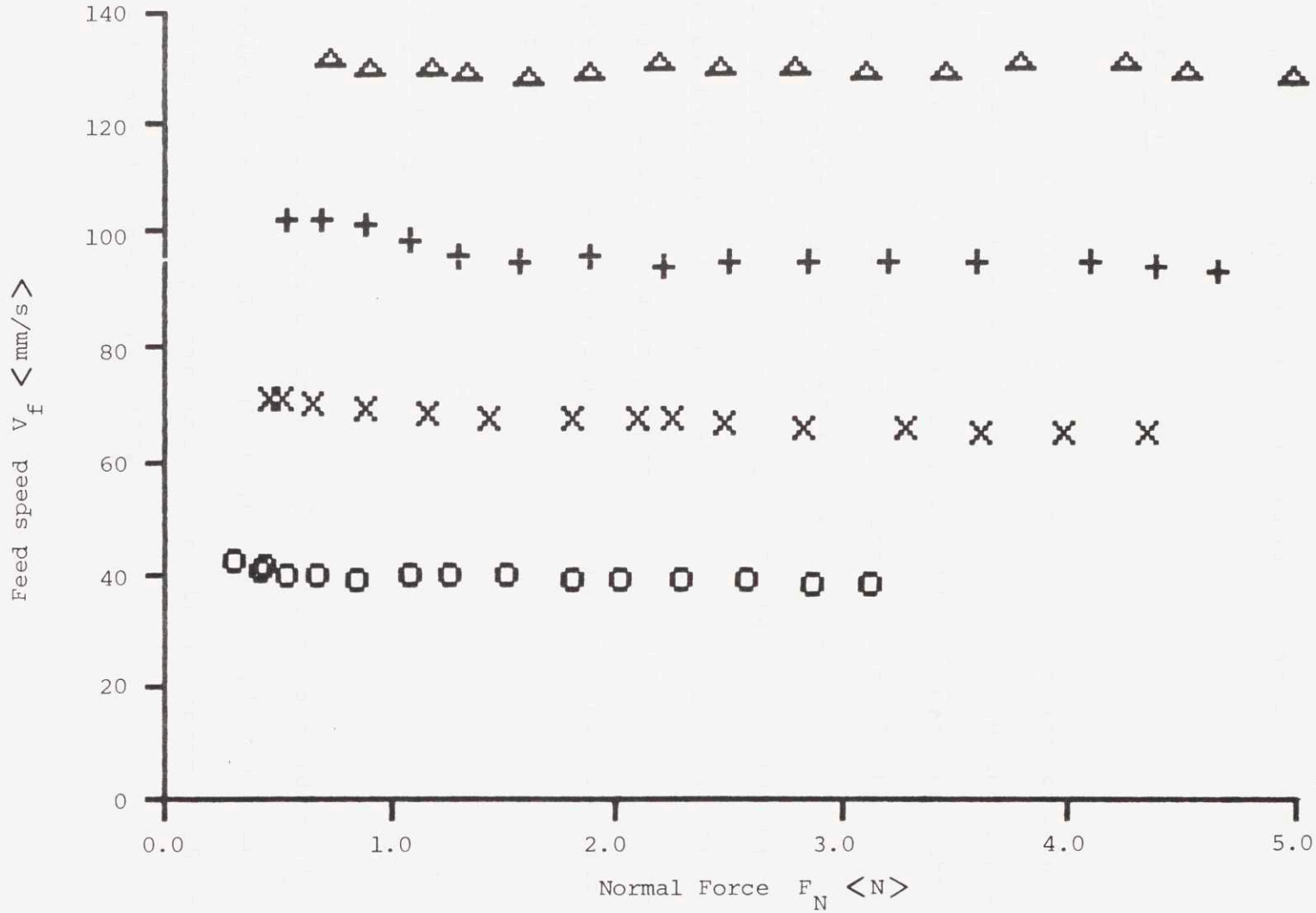

Figure 28. V_f vs. F_N with a 24-grit disk. Data show that V_f was fairly constant over the pass, while F_N changed by an order of magnitude.

Appendix D

This appendix derives an equation for the maximum temperature rise due to one grinding pass.

Background

In the grinding process, some grits are cutting metal and forming chips, while others are plowing and forming furrows but removing no metal.(D-1) In plowing, the energy goes into raising the temperature of the workpiece. In chip-forming, some of the energy goes into the chip and is removed from the workpiece. Grinding, then, causes a heat flux into the metal at the contact patch. The heat flux is assumed to be proportional to the cutting power. (Cutting power is a composite quantity which includes plowing.)

Derivation

Consider the situation of grinding a weld bead on a relatively thin plate in Figure 29a. This auto body joint consists of two plates and a structural brace held together with a silicon-bronze weld.

The time for the contact patch to pass over a point on the weld is equal to the length of the contact patch p divided by the feed speed V_f. If this time is not long, then conduction into the plate dominates any heat transfer out of the plate. The maximum temperature should occur at the back edge of the contact patch (that is, at the perimeter of the disk). Another assumption is that, in steady-state grinding, most of the heat is conducted in the direction perpendicular to the feed direction. (The forward conduction raises the temperature of the bead in front of and behind the contact patch, and lowers the temperature at the contact patch, which is moving forward. In steady state the two effects tend to cancel each other.)

The equation for the temperature distribution in a semi-infinite solid with a uniform, constant heat flux across the surface(D-2) is

$$T(x,t^*) - T_i = \frac{2q}{k}\frac{\alpha t^*}{\pi} e^{(-x^2/4\alpha t^*)} - \frac{qx}{k}\left[1 - \mathrm{erf}(x/\sqrt{4\alpha t^*})\right]$$

T - temperature at x and t* <K>

T_i - initial temperature <K>

q - heat flux across surface <W/m^2>

α - thermal diffusivity <m^2/s>

k - thermal conductivity <$W/m \cdot K$>

t^* - time during which q is applied <s>

x - direction of heat flow <m>

This equation also applies to a semi-infinite plate which has heat flux through the end face, but no heat transfer out of the plate as shown in Figure 29b. The semi-infinite plate thickness is taken to be 4t for now.

The heat flux q in the case of grinding becomes power per unit length of bead divided by the equivalent plate thickness. The maximum temperature occurs at the surface (x = 0) and after time p/V_f. Thus equation 1D is now

$$T(0,p/V_f) - T_i = \Delta T = \frac{\Pi}{2kt}\sqrt{\frac{\alpha\ p}{\pi\ V_f}} \qquad (2D)$$

in which ΔT is the maximum rise in the surface temperature along the bead due to one grinding pass.

Discussion

Plugging in typical quantities gives $\Delta T \approx 25°C$ (45°F). The actual temperature rise is probably greater by a factor of 2 or 3.

By computing the temperature distribution from equation 1D, the equivalent thickness 4t can be confirmed as a good assumption. At a distance of 25 mm from the surface in Figure 29b, the temperature rise is $(0.0001)\Delta T$. As can be seen in Figure 29a, there are 4 plate thicknesses at 25 mm from the bead (2 on each side).

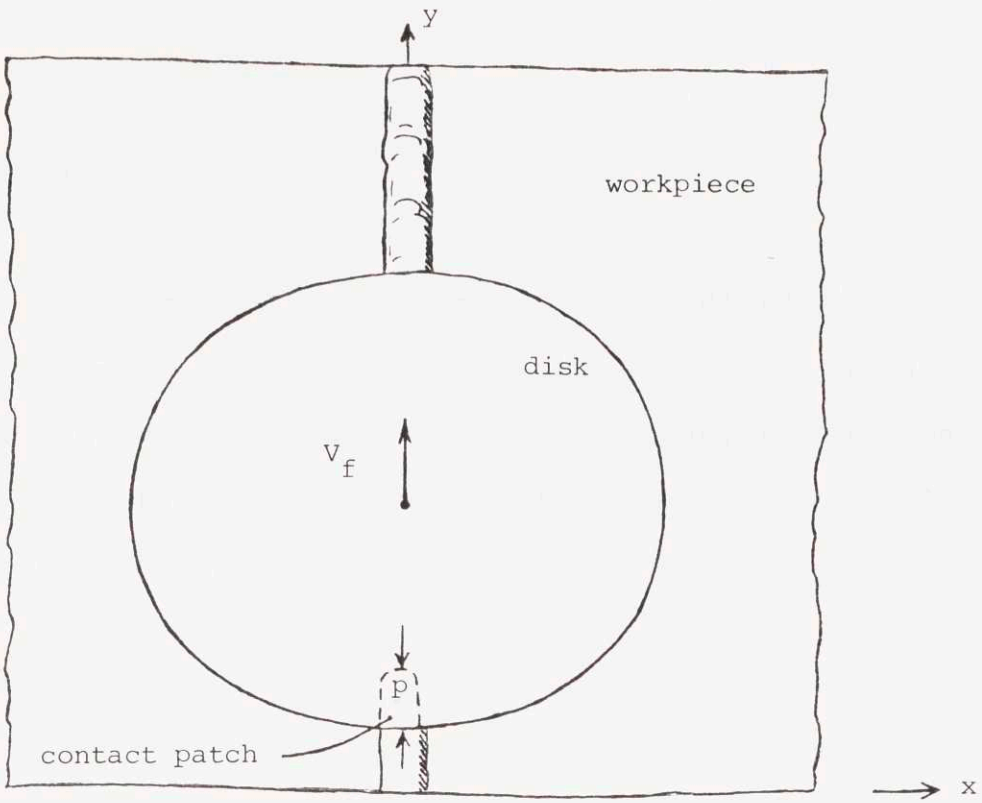

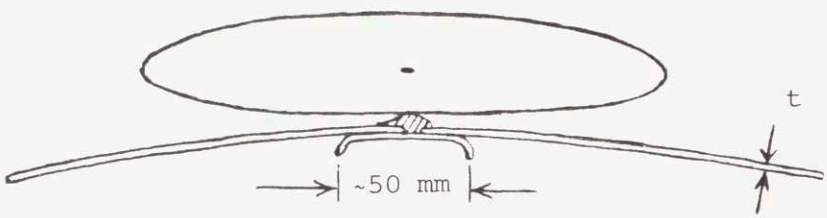

(a)

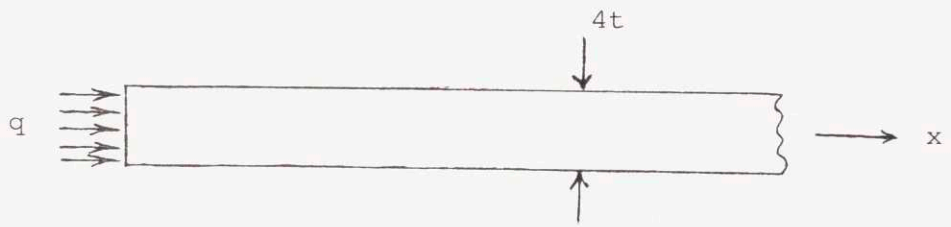

(b)

Figure 29. (a) Typical grinding situation
(b) Physical model used in ΔT derivation

Conclusion

In light of all the assumptions and simplifications that were made, we cannot expect this relation to be better than an order-of-magnitude estimate. Nevertheless, we can see the important role of the cutting power and the lesser role of the feed speed.

REFERENCES OF APPENDICES

D-1 Samuels, L. E., "The Mechanisms of Abrasive Machining", Scientific American, Vol. 239, Nov. 1978, p. 144

D-2 Incropera, F. P., DeWitt, D. P., Fundamentals of Heat Transfer, Wiley 1981, pp. 204-206